JOURNAL OF GEOPHYSICAL RESEARCH, VOL. 113, G04024, doi:10.1029/2008JG000694, 2008

Predictability of carbon emissions from biomass burning in Indonesia from 1997 to 2006

Robert D. Field[1] and Samuel S. P. Shen[2]

Received 20 January 2008; revised 26 June 2008; accepted 12 August 2008; published 5 December 2008.

[1] Drought and sea surface temperature were examined as the causes of severe biomass burning C emissions in Indonesia for 1997–2006, obtained from the Global Fire Emissions Database. Eighteen predictor variables were considered under log linear and piecewise regression models. The predictor variables considered were precipitation totals of up to 6 months, output from two soil moisture models, and sea surface temperature (SST) indicators reflecting El Niño and Indian Ocean Dipole strength. Nonparametric bootstrap techniques were used to estimate confidence intervals for predictability and thresholds below which severe C emissions are likely. Across equatorial Southeast Asia, the best predictor was 3-month total precipitation, which explained 79% of variance in C emissions. When considered individually, and with the incorporation of satellite precipitation estimates, predictability for southern Sumatra and southern Kalimantan improved to 97% and 92%, respectively, using 4-month total precipitation. There is a high risk of severe burning when 4-month precipitation falls below thresholds of 350 mm in southern Sumatra and 650 mm in southern Kalimantan and when 6-month precipitation falls below 900 mm in Papua. In general, simple precipitation totals outperformed more complicated soil moisture models and SST-based indices. Physically, seasonal precipitation controls fire emissions through its regulation of groundwater level and, hence, the amount of peat available for drying. Seasonal precipitation, in turn, is strongly influenced by SST patterns in the tropical Pacific and Indian oceans. The most severe drought and fire events appear equally influenced by Indian Ocean Dipole events and El Niño events.

Citation: Field, R. D., and S. S. P. Shen (2008), Predictability of carbon emissions from biomass burning in Indonesia from 1997 to 2006, *J. Geophys. Res.*, *113*, G04024, doi:10.1029/2008JG000694.

1. Introduction

[2] The interannual growth of CO_2 and other greenhouse gases is not steady but occurs irregularly over timescales of 2–5 years, with biomass burning proposed as the main source of this interannual growth [*Langenfelds et al.*, 2002]. *Zeng et al.* [2005] estimated that biomass burning represents roughly 20% of the mean interannual carbon flux anomaly, mainly through the increase in tropical fires in response to drought conditions. Indonesian biomass burning in 1997 was estimated to constitute 15–40% of the mean annual global C emissions from fossil fuel burning [*Page et al.*, 2002]. *Podgorny et al.* [2003] quantified the climatic impacts of the 1997 event, estimating that aerosol emissions from the fires resulted in at least a 50% increase in atmospheric solar heating within the first three vertical kilometers and at least a 15% reduction in seasonal mean solar radiation incident at the surface of the equatorial Indian Ocean. The serious health impacts of transboundary haze generated by Indonesian fires have also been documented [*Sastry*, 2002; *Kunii et al.*, 2002].

[3] With industrial logging and agriculture as the underlying causes [*Dennis et al.*, 2005; *Langner et al.*, 2007], the trigger for severe fire and haze episodes in Indonesia is drought. There is significant interannual variability in dry season rainfall over Indonesia, due to changes in ocean and atmospheric circulation in the tropical Pacific and Indian oceans. In the Pacific, the anomalously high sea surface temperatures (SST) appear in the east, weakening the Walker circulation and resulting in a reduced pooling of warm water and convection in the western Pacific [*Gutman et al.*, 2000; *Hendon*, 2003]. Over Indonesia, this results in a pronounced decrease in rainfall during the dry seasons, as convection shifts eastward into the central Pacific. Similar impacts also result from SST anomalies in the Indian Ocean, where precipitation shifts northwestward away from western Indonesia [*Saji et al.*, 1999]. During these periods, burning escapes control, igniting vast deposits of peat soils, whose water holding capacity has been reduced because of extensive draining [*Page et al.*, 2002; *Usup et al.*, 2004]. The provinces of Riau, Jambi, and South Sumatra on the island of Sumatra and West, Central, South and East Kalimantan are the main fire prone regions of Indonesia [*Heil and Goldammer*, 2001].

[1]Department of Physics, University of Toronto, Toronto, Ontario, Canada.
[2]Department of Mathematics and Statistics, San Diego State University, San Diego, California, USA.

0148-0227/08/2008JG000694$09.00

[4] Because of the large amounts of smoke produced, the haze signature of the fires is seen clearly in different proxy measurements, which have also been used to understand underlying causes of the fires. *Field et al.* [2004] showed that reductions in visible range at airports in Sumatra and Kalimantan during 1994–1998 could be explained by anomalously low values of a drought code used for fire danger monitoring in boreal and temperate forests. Over a longer period from 1973 to 2003, *Wang et al.* [2004] showed that reductions in visible range over Sumatra were in phase with warm ENSO periods in 1982/1983, 1987/1988, 1991/1992, 1994/1995, 1997/1998 and 2002/2003, as indicated by the Niño3.4 SST index.

[5] *Kita et al.* [2000] and *Thompson et al.* [2001] also showed qualitatively that enhancements of the Total Ozone Mapping Spectrometer Aerosol Index (TOMS AI) over Indonesia have occurred during the El Niño episodes of 1982/1983, 1987/1988 and 1991/1992 and 1997/1998, also using SSTs as an explanatory variable. Severe burning was also observed more recently in 2006 [*Lohman et al.*, 2007], and elevated CO and O_3 measurements from the Tropospheric Emission Spectrometer (TES) and Measurements of Pollution in the Troposphere (MOPITT) instruments were attributed to Indonesian fires, and ultimately to El Niño-induced drought [*Logan et al.*, 2008]. These atmospheric indicators provide useful longer-term characterizations of smoke but are complicated by several factors. Visible range data is a useful surface indicator, but is somewhat subjective in that it records maximum distance seen by a human observer. The TOMS sensor and AI retrieval algorithm have limited detection ability in the lower troposphere [*Herman et al.*, 1997], resulting in underdetection problems and a lag between the onset of severe haze and its detection. It is also difficult to attribute observed atmospheric haze to a specific origin, due to transport and mixing of smoke from different sources.

[6] Satellite-detected hot spots are the best available fire indicator for many regions of the world [*Duncan et al.*, 2003] and provide a means for quantifying the underlying causes of fire, especially in regions such as Indonesia which lack systematic aerial estimates of burned area. Over Indonesia, *Sudiana et al.* [2003] assessed the relationship between AVHRR hot spot occurrence from 1981 to 1993, showing qualitatively that fire episodes occurred under dryer conditions, as reflected by a fire danger index calibrated for North American conditions.

[7] *van der Werf et al.* [2008] examined the relationship between climate and fire over the entire tropics and subtropics using TRMM fire counts. Using an index of fire potential based on dry season length and total dry season precipitation, they showed that fire in some regions of Indonesia was correlated with high fire potential, and that high fire count years were associated with anomalously low dry season rainfall. Other studies using satellite-detected hot spots in Indonesia have shown that fire occurrence is related to land use [*Stolle and Lambin*, 2003] and occurs under dryer conditions associated with El Niño conditions [*Dymond et al.*, 2005; *Fuller and Murphy*, 2006].

[8] The goal of this study was to better understand climatic factors contributing to biomass burning emissions in Indonesia. Specifically, we tried to identify, from among a broad pool, climate variables which explain the highest proportion of variance in direct C emissions from biomass burning over Indonesia, as estimated from the Global Fire Emissions Database of *van der Werf et al.* [2006], for 1997 to 2006. Particular attention was devoted to interregional variability of emissions and predictability, and the degree to which drought thresholds could be identified for improved interpretation of seasonal rainfall forecasts. Formal quantitative estimates of proportion of variance in fire occurrence explained by climate predictor variables have been limited to *Field et al.* [2004] and *Fuller and Murphy* [2006]. Given the potential application of such predictor variables in seasonal prediction or in climate change outlooks, detailed assessments of the uncertainty of predictions were also made.

2. Data and Methods

2.1. The Global Fire Emissions Database

[9] Estimates of biomass burning emissions over Indonesia were obtained from the Global Fire Emissions Database (GFED) [*van der Werf et al.*, 2006], which is currently the best available source of global fire emissions data. The data is available on a 1° by 1° grid for the period 1997–2006 at monthly temporal resolution. Fire occurrence and area burned are determined from cross-calibrated ATSR, TRMM, and MODIS hot spot counts. Emissions estimates are based on fuel load predictions from a global vegetation model, a soils map for subsurface fuels, and emissions factors specific to different combustion products. Over Indonesia, an important distinction is also made between organic soils and nonburning mineral soils. Following *Page et al.* [2002] and *van der Werf et al.* [2006], we used direct carbon (C) emissions as our emissions indicator.

[10] Previous case studies have shown that the seasonality of fire emissions can vary considerably across Indonesia. The 1998 fires in East Kalimantan during February to April 1998, for example, were decoupled from the 1997 July–November burning across the rest of Kalimantan [*Heil and Goldammer*, 2001; *Siegert and Hoffmann*, 2000] and occurred under localized drought conditions not seen in other parts of Kalimantan [*Field et al.*, 2004]. To identify Indonesia's main seasonal burning regions, a spatial principal component analysis was performed to identify regions of coherent seasonal burning, similar to the approach of *Gedalof et al.* [2005]. Each region was then analyzed individually to identify possible climatic drivers.

2.2. Climatic Indices

[11] We considered a broad range of variables in trying to predict severe biomass burning. Following *Fuller and Murphy* [2006], we used the sea level-pressure-based Southern Oscillation Index and sea surface temperature-based Niño3.4 index as indicators of El Niño strength. In addition, we considered the Multivariate ENSO Index (MEI) [*Wolter and Timlin*, 1993] and the recently developed Dipole Mode Index (DMI) of *Saji et al.* [1999]. The MEI is a hybrid index incorporating the SLP behavior of the SOI and the SST behavior of the Niño3.4. The DMI measures the strength of the Indian Ocean Dipole events, whereby anomalies appearing in the basin are related to anomalously low precipitation in Indonesia.

[12] To examine the direct relationship between drought and fire in Indonesia, we considered two different precipitation data sets and two soil moisture models, all of which have global coverage and monthly temporal resolution. The NCEP Precipitation over Land (PRECL) data set [*Chen et al.*, 2002] was the simplest data set considered, consisting of rain gauge only measurements interpolated onto a 2.5° × 2.5° grid. The Global Precipitation Climatology Project (GPCP) data set [*Adler et al.*, 2003] uses gauge data, but also incorporates infrared and microwave satellite retrievals. The incorporation of satellite data was warranted for inclusion in this analysis given the sparse rain gauge coverage over much of Indonesia. To distinguish between single months with anomalously low precipitation and persistent seasonal drought, precipitation totals for up to 6 months prior were considered as individual drought indices.

[13] Given the significant contribution of peat burning to emissions, we also examined output from two soil moisture models as predictor variables. The National Centre for Environmental Prediction Global Soil Moisture (SOILM) data set of *Fan and van den Dool* [2004] is based on a simple single bucket moisture model. Although the data are available globally, model parameters are based on field studies in the U.S. Great Plains, and currently with no parameter variation across soil or land cover types. As input, the model uses the monthly precipitation data from PRECL, and surface air temperature data from the NCEP-NCAR reanalysis [*Kalnay et al.*, 1996]. Data are distributed at a 0.5 by 0.5 spatial resolution, but have an effective resolution of 2.5° × 2.5° corresponding to that of the PRECL data set.

[14] The Palmer Drought Severity Index (PDSI) computed globally by *Dai et al.* [2004] was also considered. Like the SOILM model, the PDSI was designed mainly for agricultural applications in the U.S., to measure the cumulative departure in moisture supply and loss at the surface, but has been applied in numerous other applications, including historical forest fire and climate analyses [*Westerling et al.*, 2002; *Hessl et al.*, 2004]. It is an anomaly based index, in that local climatological means of rainfall are included as moisture parameters, and is cumulative, with the current month's PDSI a function of the current month's weather and last month's PDSI.

[15] The PDSI uses a two-layer soil model, and unlike the SOILM model, does distinguish between the water holding capacity of different soil types. PDSI values are on a standardized scale, with a minimum of −10 corresponding to severe moisture deficit and a maximum of +10 corresponding to a moisture surplus. The technical details of the PDSI are described by *Ntale and Gan* [2003]. Unlike the SOILM model, the PDSI has undergone some validation against field data outside of the U.S., showing strong correlation with measured soil moisture in southern China and streamflow in Brazil and the Congo, particularly compared with raw rainfall measurements [*Dai et al.*, 2004].

[16] In total, 18 predictor variables were considered, including the 1- to 6-month back totals for each of the precipitation indices.

2.3. Threshold Estimation

[17] Although there is a regular wet and dry season cycle driven by the Asian-Australian monsoon, it is only during anomalously dry years that fires are a serious problem. *Field et al.* [2004] showed this to be the case over the period from 1994 to 1999, when there were severe haze events during the dry seasons of the 1994 and 1997 El Niño years, but a near absence of haze events during the other non El Niño years. Their analysis showed that the absence of haze during non El Niño years corresponded to a moisture threshold above which conditions are too wet to support extensive biomass burning and haze.

[18] Presumably, this threshold corresponds to a moisture threshold in vegetation and organic soil, which is supported by experimental data. *Frandsen* [1997] found this to be the case in a series of experimental burns for different organic soils across North America, showing that the probability of ignition increases below a moisture content of 120% for the majority of soil types, and with a higher threshold for soil types with a higher inorganic content. In Indonesia, *de Groot et al.* [2005] showed that dead "alang-alang" grass, a key surface fuel type leading to subsurface fires, had a moisture content ignition threshold of 27.8%. Moisture content in Indonesian peatlands will begin to decrease when the groundwater level falls below the surface and the peat is exposed to unsaturated air.

[19] Piecewise regression was used to estimate the relationship between drought and emissions in such a way as to explicitly include an estimate of drought threshold. The model consists of two linear segments, constrained to be equal at an unknown change point which is interpreted as the threshold value in this context. Using the formulation of *Toms and Lesperance* [2003], the model is given by

$$f(x) = \begin{cases} \beta_0 + \beta_1 x, & x \le \alpha \\ \beta_0 + \beta_1 x + \beta_2 (x - \alpha), & x > \alpha \end{cases} \quad (1)$$

where α is the change point to be estimated, β_1 is the slope of the line below the change point and $\beta_1 + \beta_2$ is the slope of the second line, x is a given predictor variable, and $f(x)$ is the emissions. This formulation constrains continuity between the two model sections at α, which provides a less ambiguous threshold estimate than the curvature-based approach of *Field et al.* [2004]. The model was estimated through straightforward use of nonlinear fitting routines. For a comparison to *Fuller and Murphy* [2006], basic log-transformed relationships were also considered for each variable and analysis region, which implicitly models the drought-emissions relationship in a nonlinear fashion. Drought-emissions relationships were examined individually for each subregion region identified through the principal component analysis, rather than the analysis of *Field et al.* [2004] or *Dymond et al.* [2005], who aggregated data across all of Sumatra and Kalimantan, and *Fuller and Murphy* [2006], who focused on the entire Indonesian archipelago.

[20] Ultimately, we wished to identify the moisture index which best predicted serious emissions episodes, and which separated severe drought from normal conditions. The performance of different models and predictor variables was evaluated using the coefficient of determination (R^2). To estimate a confidence interval for R^2 and threshold statistics, we used a fully nonparametric bootstrapping approach [*Efron and Tibshirani*, 1993]. Using this method, the random samples of pairs (x_i, y_i) are drawn with replace-

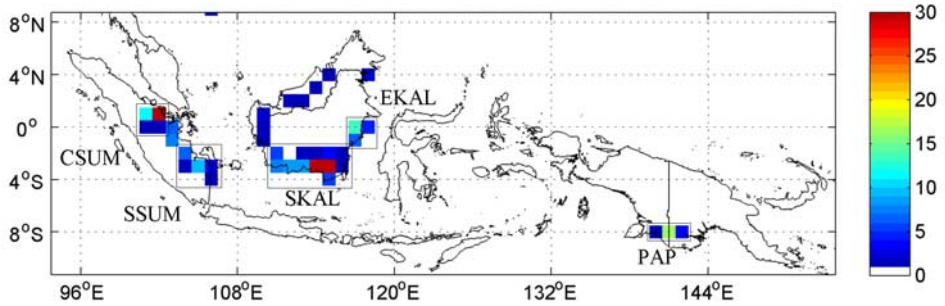

Figure 1. Mean annual C emissions (Tg), 1997–2006, and the five burning regions considered within the EQSA domain. Regional names do not correspond to province names.

ment from the original sample, rather than resampling the residuals, which is more sensitive to the underlying distribution of error terms. The change point function (1) was fit to each random sample, yielding a distribution of R^2 and $\hat{\alpha}$ estimates for each model. 95% confidence intervals for the estimates were obtained from the 2.5th and 97.5th percentiles of the bootstrapped distributions. For each moisture index and region, a total of 1000 resamples were drawn.

3. Results

3.1. Emissions Characteristics

[21] Figure 1 shows the mean annual C emissions across all of Indonesia, during the 1997–2006 period, calculated from the GFED data set [*van der Werf et al.*, 2006]. The spatial principal component analysis yielded five main regions where C emissions tended to covary (Figure 2) within the entire Indonesian region (EQSA, for equatorial Southeast Asia): central Sumatra (CSUM), southern Sumatra (SSUM), southern Kalimantan (SKAL), eastern Kalimantan (EKAL) and Papua (PAP). Figure 2a shows the spatial loadings of the first EOF, which is a dominant mode of burning during the southeast monsoon dry season, and coincides with the primary precipitation zone of *Aldrian and Susanto* [2003]. Figure 2b shows the second EOF, which mainly reflects the early 1998 burning in EKAL. Figure 2b shows the third EOF, which is dominated by early season burning in 2002, 2005, and 2006 in CSUM. The first three EOFs explain 59%, 12%, and 10% of the variability in C emissions, respectively.

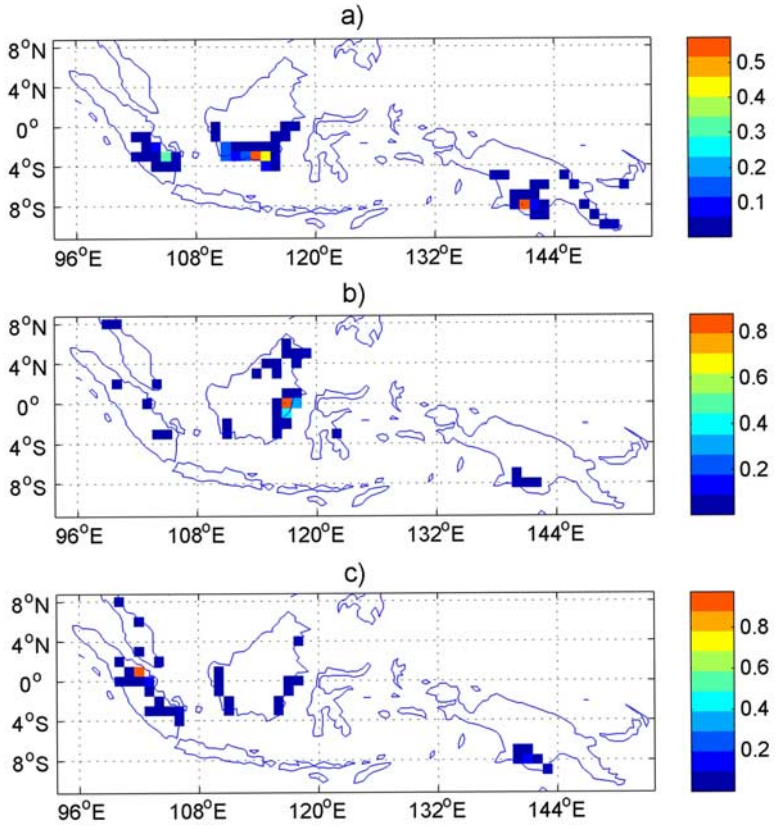

Figure 2. (a) First, (b) second, and (c) third EOF patterns of C emissions.

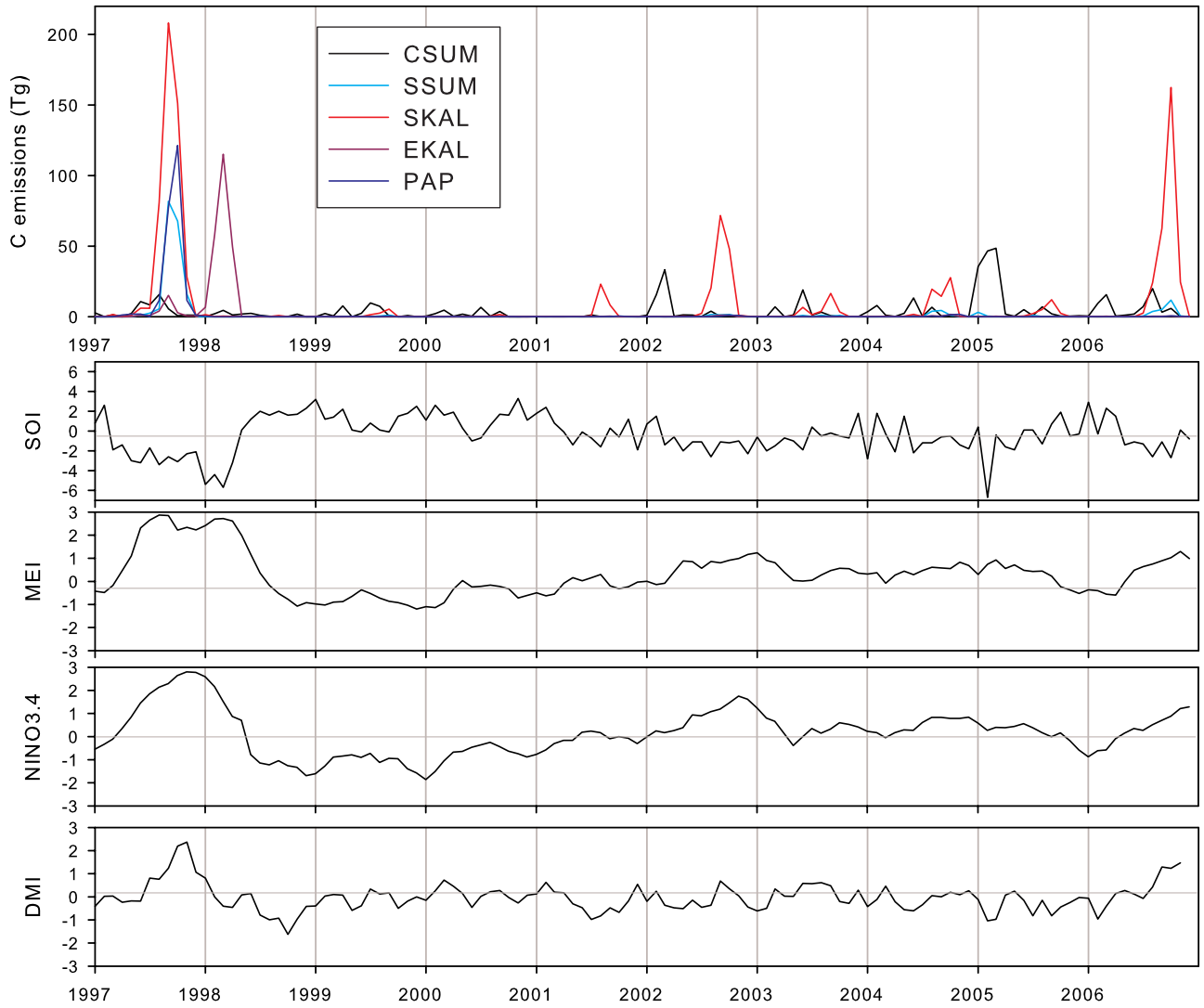

Figure 3. (top) Monthly emissions for analysis regions and (bottom) SOI, MEI, Niño3.4, and DMI indices.

[22] C emissions in each region were marked by large interannual differences (Figure 3). The 1997 event was by far the biggest during the analysis period, with 960 Tg emitted across all analysis regions during the burning from June through November. Of the total emissions during this event, 50% came from SKAL, 24% from PAP, and 18% from SSUM, with minor contributions from CSUM and EKAL. The 1998 episode lasted from February until April; 96% of the 231 Tg total emissions was from EKAL, with minor contributions from CSUM. The period from 1999 to 2001 was characterized by only minor emissions totaling 104 Tg over the 3 years, marked only by a 35 Tg event in SKAL during June to September 2001. This was followed by emissions of 212 Tg in 2002, which occurred during two isolated episodes: a 49 Tg event during February and March restricted entirely to the CSUM region, followed by a 153 Tg event from August to November in SKAL.

[23] Similar to the previous year, there were smaller isolated events in 2003: 19 Tg during June in CSUM and 32 Tg in SKAL from June until September. Emissions in 2004 were dominated by a 62 Tg event from August until November in SKAL, preceded by 13 Tg of emissions in CSUM during June. In 2005, there was a large 130Tg event in CSUM from January until March, with a near absence of fire in other regions.

[24] In 2006, there were 25 Tg of emissions in CSUM during February and March, but burning was dominated by the 274 Tg of emissions from August to November in SKAL, over half of which occurred during October. During

Table 1. Analysis Regions and Abbreviations

Region	Abbreviation
Equatorial Southeast Asia	EQSA
Central Sumatra	CSUM
Southern Sumatra	SSUM
Southern Kalimantan	SKAL
Eastern Kalimantan	EKAL
Papua	PAP

Table 2. Regression Summary Statistics for EQSA Region[a]

	Log Linear R^2	Piecewise R^2	Piecewise α
SOI	0.27 (0.15, 0.40)	0.22 (0.11, 0.41)	−0.7 (−1.9, 0.7)
MEI	0.32 (0.19, 0.45)	0.43 (0.20, 0.86)	−20 (−2.7, −0.5)
NIÑO34	0.28 (0.14, 0.41)	0.33 (0.15, 0.72)	−1.2 (−2.9, 0.2)
DMI	0.09 (0.01, 0.23)	0.40 (0.12, 0.78)	−0.3 (−1.1, −0.1)
GPCP	0.52 (0.37, 0.65)	0.78 (0.31, 0.92)	109 (92, 128)
GPCP2	0.47 (0.32, 0.60)	0.81 (0.27, 0.94)	203 (169, 207)
GPCP3	0.41 (0.27, 0.53)	0.54 (0.26, 0.86)	437 (295, 527)
GPCP4	0.31 (0.18, 0.45)	0.39 (0.21, 0.82)	626 (481, 794)
GPCP5	0.27 (0.14, 0.41)	0.37 (0.15, 0.76)	734 (480, 978)
GPCP6	0.24 (0.12, 0.38)	0.35 (0.17, 0.69)	916 (631, 1027)
PRECL	0.50 (0.36, 0.63)	0.49 (0.25, 0.84)	142 (103, 168)
PRECL2	0.42 (0.28, 0.55)	0.81 (0.23, 0.94)	257 (244, 265)
PRECL3	0.35 (0.21, 0.50)	0.79 (0.34, 0.90)	413 (379, 456)
PRECL4	0.25 (0.12, 0.39)	0.20 (0.10, 0.30)	NA
PRECL5	0.19 (0.08, 0.32)	0.49 (0.14, 0.85)	784 (609, 883)
PRECL6	0.15 (0.05, 0.27)	0.37 (0.12, 0.77)	980 (786, 1099)
SOILM	0.32 (0.19, 0.46)	0.60 (0.22, 0.88)	343 (307, 364)
PDSI	0.31 (0.18, 0.46)	0.28 (0.15, 0.52)	−2 (−2, −1)

[a] R^2 values for log linear fit, R^2 values for piecewise fit, threshold estimate α for piecewise fit. Values in parentheses indicate bootstrap-derived 95% confidence intervals. NA, not available.

this period, there was also 36 Tg of emissions from CSUM and 21 Tg of emissions from SSUM. These combined events led to 2006 being the second-largest emissions year, after 1997.

[25] Over the analysis period, the SKAL region was the biggest source of emissions, constituting 39% of emissions in EQSA during 1997 to 2006, and driving the anomalously high emissions during 1997, 2002, and 2006. The CSUM region represented the 17% of the emissions, which often occurred during the first 3 months of a year, decoupled from the emissions in other regions, such as SKAL, where burning occurred only in June–November. The remainder of the total emissions was split evenly across SSUM (8%), EKAL (12%), and PAP (11%), which occurred primarily as single large pulses in 1997 and 1998, with only minor contributions at other times. These five areas together represented 82% of emissions within the EQSA regions.

3.2. Prediction Across All of Indonesia

[26] Table 1 shows that across the entire EQSA region and among the 18 predictor variables, the MEI under the piecewise model was the best climate-based predictor, with $R^2 = 0.43$, but the performance of the DMI was comparable with $R^2 = 0.40$, hence SST variability is a better predictor than SLP variability. Indeed, the SST indices are more robust climate indicators, being spatially integrated over a broad region, compared to the SOI which is based on the SLP variations at two individual sites. Although a strong quantitative relationship appears not to exist, a general correspondence between emissions and SST variability is apparent from Figure 3. The large 1997 and 1998 events occurred under exceptionally strong El Niño conditions, as indicated by the Niño3.4 and MEI and also with an Indian Ocean Dipole event indicated by the DMI. From the second half of 1998 until 2001, neutral or La Niña conditions persisted, during which severe fire occurrence was absent. The elevated emissions in 2002 and 2006 appeared to occur under El Niño conditions, as indicated by the MEI. The 2006 event also occurred under positive DMI conditions.

[27] Improvements in predictability were obtained by considering drought conditions across EQSA, rather than the ENSO or DMI indices. The best results were obtained with the piecewise linear model, under which the PRECL3 was identified as the best predictor with $R^2 = 0.79$. Figure 4 shows the time series of EQSA C emissions and PRECL3, with the estimated threshold of 413 mm also plotted. The PRECL2, GPCP and GPCP2 indices yielded comparable levels of predictability, but with slightly wider confidence intervals. The significant burning events in the dry seasons of 1997, 2002, and 2006 all occurred below threshold values, with a very fine separation between these years and the only moderately dry years of 2001 and 2004. The significant EKAL burning in 1998 occurred under EQSA-wide PRECL3 conditions well above the estimated threshold range, owing to the highly localized nature of the drought in EKAL.

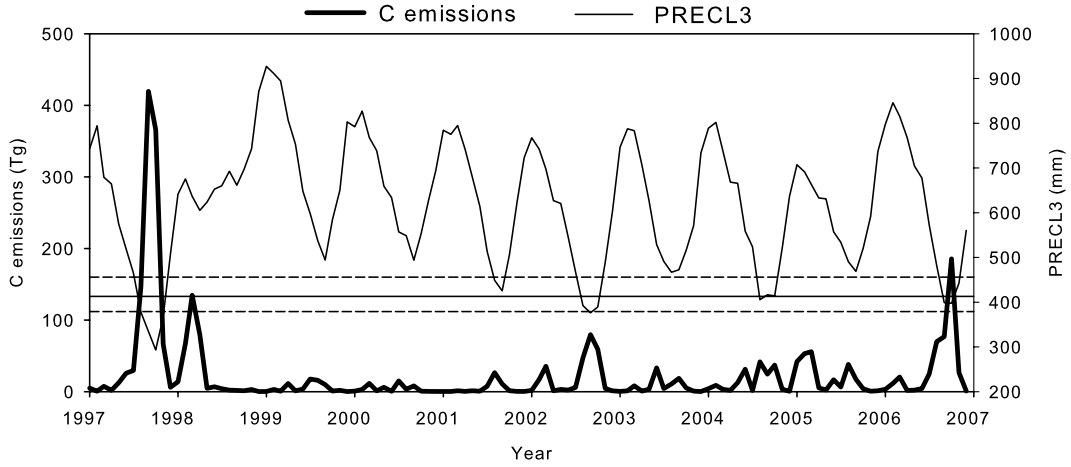

Figure 4. EQSA monthly C emissions and PRECL3. The solid horizontal line is the threshold estimate, and the dashed lines are 95% confidence intervals.

Table 3. Regression Summary Statistics for CSUM Region[a]

	Log Linear R^2	Piecewise R^2	Piecewise α
SOI	0.04 (0.00, 0.14)	0.23 (0.00, 0.62)	−5.7 (−5.8, −5.6)
MEI	0.02 (0.00, 0.09)	0.02 (0.00, 0.07)	−0.7 (−3.2, 2.6)
NIÑO34	0.00 (0.00, 0.04)	0.04 (0.01, 0.08)	−0.3 (−0.6, 0.7)
DMI	0.01 (0.00, 0.05)	0.06 (0.00, 0.57)	0.5 (−0.2, 3.1)
GPCP	0.35 (0.23, 0.48)	0.19 (0.10, 0.41)	221 (136, 286)
GPCP2	0.39 (0.23, 0.53)	0.22 (0.10, 0.45)	431 (317, 567)
GPCP3	0.29 (0.16, 0.43)	0.11 (0.03, 0.26)	782 (535, 1076)
GPCP4	0.17 (0.06, 0.30)	0.03 (0.00, 0.09)	772 (288, 2385)
GPCP5	0.09 (0.02, 0.20)	0.01 (0.00, 0.05)	1085 (708, 2307)
GPCP6	0.06 (0.01, 0.15)	0.02 (0.00, 0.06)	1300 (1047, 1879)
PRECL	0.27 (0.15, 0.42)	0.07 (0.02, 0.19)	122 (−144, 487)
PRECL2	0.20 (0.09, 0.34)	0.06 (0.01,0.14)	371 (117, 927)
PRECL3	0.12 (0.04, 0.23)	0.03 (0.01, 0.08)	687 (591, 1044)
PRECL4	0.04 (0.00, 0.14)	0.00 (0.00, 0.03)	NA
PRECL5	0.01 (0.00, 0.07)	0.01 (0.00, 0.07)	1150 (719, 1848)
PRECL6	0.00 (0.00, 0.03)	0.00 (0.00, 0.03)	NA
SOILM	0.01 (0.00, 0.06)	0.01 (0.00, 0.04)	NA
PDSI	0.06 (0.01, 0.13)	0.07 (0.03, 0.13)	−3 (−5, −2)

[a] R^2 values for log linear fit, R^2 values for piecewise fit, threshold estimate α for piecewise fit. Values in parentheses indicate bootstrap-derived 95% confidence intervals. NA, not available.

Table 5. Regression Summary Statistics for SKAL Region[a]

	Log Linear R^2	Piecewise R^2	Piecewise α
SOI	0.08 (0.01, 0.19)	0.10 (0.05, 0.18)	−3.1 (−3.4, −2.6)
MEI	0.16 (0.05, 0.30)	0.18 (0.04, 0.67)	−0.1 (−2.7, 2)
NIÑO34	0.19 (0.08, 0.33)	0.23 (0.06, 0.55)	−0.3 (−1.8, 1.4)
DMI	0.16 (0.04, 0.31)	0.44 (0.20, 0.76)	−0.2 (−0.8, 0.1)
GPCP	0.38 (0.23, 0.53)	0.20 (0.11, 0.31)	603 (603, 603)
GPCP2	0.58 (0.43, 0.70)	0.63 (0.36, 0.92)	306 (160, 356)
GPCP3	0.70 (0.57, 0.80)	0.88 (0.75, 0.97)	411 (275, 465)
GPCP4	0.67 (0.55, 0.77)	0.92 (0.74, 0.98)	595 (472, 656)
GPCP5	0.56 (0.41, 0.68)	0.69 (0.44, 0.91)	882 (688, 1121)
GPCP6	0.42 (0.27, 0.55)	0.47 (0.25, 0.78)	1281 (978,1573)
PRECL	0.52 (0.40, 0.63)	0.40 (0.25, 0.63)	119 (66, 162)
PRECL2	0.66 (0.55, 0.74)	0.61 (0.42, 0.92)	186 (69, 282)
PRECL3	0.67 (0.56, 0.77)	0.71 (0.50, 0.92)	275 (219, 365)
PRECL4	0.59 (0.46, 0.70)	0.69 (0.49, 0.90)	427 (278, 502)
PRECL5	0.49 (0.35, 0.61)	0.27 (0.17, 0.37)	NA
PRECL6	0.38 (0.25, 0.52)	0.23 (0.13, 0.34)	NA
SOILM	0.69 (0.57, 0.77)	0.70 (0.50, 0.91)	488 (418, 519)
PDSI	0.14 (0.04, 0.26)	0.10 (0.03, 0.19)	−4 (−18, 12)

[a] R^2 values for log linear fit, R^2 values for piecewise fit, threshold estimate α for piecewise fit. Values in parentheses indicate bootstrap-derived 95% confidence intervals. NA, not available.

3.3. Subregional Prediction

[28] The results for the subregional analyses are listed in Tables 2–7. In CSUM, none of the climate indices showed any well-constrained predictive power under either of the log linear or piecewise models (Table 3). The best performing drought predictor was GPCP2 under a log linear model, with $R^2 = 0.39$. The precipitation predictors were similar to the EQSA region in that predictability decreased as the precipitation back totaling periods increased beyond 2 months, suggesting a shorter drought memory with respect to biomass burning emissions. For CSUM, the best piecewise predictor was GPCP2 with an R^2 of 0.22, and so the piecewise model offered no improvement over the log linear model, nor did the PDSI or SOILM indices. The GPCP2 and C emissions for CSUM are shown in Figure 5 along with the estimated threshold range. Although the piecewise model provided less predictability over CSUM than the EQSA region, the 3 most significant emissions episodes in 1997, early 2002, and early 2005 did occur under GPCP2 conditions below the lower estimated confidence limit of 317 mm, suggesting some correspondence, albeit more complicated, between precipitation and C emissions.

[29] In contrast to CSUM, the predictability for the SSUM region improved compared to the whole EQSA region (Table 4). The best log linear predictors were the GPCP2 and GPCP3 variables, and again, the predictability for both rainfall-based totals decreased with a longer back totaling period. The fitted piecewise models had higher R^2 values, but as in the case for EQSA, were less

Table 4. Regression Summary Statistics for SSUM Region[a]

	Log Linear R^2	Piecewise R^2	Piecewise α
SOI	0.14 (0.05, 0.27)	0.07 (0.02, 0.23)	−0.2 (−2.1, 3.3)
MEI	0.24 (0.09, 0.41)	0.31 (0.08, 0.97)	−1.2 (−2.7, −0.3)
NIÑO34	0.24 (0.08, 0.40)	0.35 (0.09, 0.96)	−1.5 (−2.8, −1)
DMI	0.21 (0.06, 0.39)	0.50 (0.17, 0.99)	−0.6 (−1.5, −0.2)
GPCP	0.47 (0.30, 0.61)	0.84 (0.09, 0.99)	62 (36, 73)
GPCP2	0.64 (0.46, 0.76)	0.93 (0.17, 0.99)	121 (108, 168)
GPCP3	0.65 (0.46, 0.77)	0.94 (0.31, 1.00)	223 (179, 290)
GPCP4	0.59 (0.43, 0.72)	0.97 (0.64, 1.00)	317 (290, 361)
GPCP5	0.52 (0.36, 0.66)	0.83 (0.21, 0.99)	468 (358, 564)
GPCP6	0.46 (0.30, 0.60)	0.58 (0.16, 0.99)	734 (392, 858)
PRECL	0.47 (0.33, 0.60)	0.97 (0.12, 1.00)	22 (22, 25)
PRECL2	0.59 (0.41, 0.72)	0.94 (0.19, 0.99)	75 (64, 101)
PRECL3	0.57 (0.39, 0.71)	0.92 (0.35, 1.00)	170 (118, 267)
PRECL4	0.51 (0.34, 0.64)	0.95 (0.61, 1.00)	240 (187, 363)
PRECL5	0.42 (0.26, 0.57)	0.73 (0.33, 0.99)	466 (251, 578)
PRECL6	0.34 (0.18, 0.49)	0.41 (0.11, 0.98)	774 (458, 983)
SOILM	0.61 (0.43, 0.74)	0.92 (0.22, 1.00)	440 (401, 486)
PDSI	0.15 (0.04, 0.30)	0.09 (0.02, 0.19)	4 (4, 4)

[a] R^2 values for log linear fit, R^2 values for piecewise fit, threshold estimate α for piecewise fit. Values in parentheses indicate bootstrap-derived 95% confidence intervals.

Table 6. Regression Summary Statistics for EKAL Region[a]

	Log Linear R^2	Piecewise R^2	Piecewise α
SOI	0.24 (0.08, 0.43)	0.35 (0.08, 0.99)	−2.1 (−3.3, −0.4)
MEI	0.40 (0.20, 0.55)	0.46 (0.23, 1.00)	−2.2 (−2.7, −1.6)
NIÑO34	0.27 (0.12, 0.41)	0.08 (0.02, 0.22)	7.7 (7.7, 7.7)
DMI	0.10 (0.02, 0.26)	0.01 (0.00, 0.18)	−0.5 (−3.7, 2.3)
GPCP	0.43 (0.28, 0.56)	0.34 (0.03, 0.96)	84 (21, 106)
GPCP2	0.60 (0.47, 0.71)	0.58 (0.12, 1.00)	171 (81, 293)
GPCP3	0.61 (0.48, 0.71)	0.46 (0.08, 1.00)	298 (193, 573)
GPCP4	0.55 (0.42, 0.66)	0.22 (0.07, 0.85)	637 (375, 826)
GPCP5	0.47 (0.30, 0.60)	0.20 (0.08, 0.72)	833 (597, 1010)
GPCP6	0.41 (0.24, 0.56)	0.28 (0.12, 0.87)	956 (728, 1085)
PRECL	0.29 (0.15, 0.43)	0.02 (0.00, 0.10)	NA
PRECL2	0.37 (0.23, 0.52)	0.02 (0.01, 0.30)	252 (−23, 906)
PRECL3	0.35 (0.22, 0.51)	0.02 (0.00, 0.14)	467 (NA)
PRECL4	0.31 (0.19, 0.47)	0.02 (0.00, 0.11)	721 (NA)
PRECL5	0.28 (0.16, 0.44)	0.01 (0.00, 0.14)	1487 (905, 1911)
PRECL6	0.28 (0.15, 0.42)	0.03 (0.01, 0.10)	NA
SOILM	0.55 (0.40,0.67)	0.27 (0.06, 0.91)	519 (428, 575)
PDSI	0.32 (0.11, 0.54)	0.52 (0.07, 1.00)	−5 (−6, −3)

[a] R^2 values for log linear fit, R^2 values for piecewise fit, threshold estimate α for piecewise fit. Values in parentheses indicate bootstrap-derived 95% confidence intervals. NA, not available.

Table 7. Regression Summary Statistics for PAP Region[a]

	Log Linear R^2	Piecewise R^2	Piecewise α
SOI	0.05 (0.00, 0.19)	0.06 (0.02, 0.15)	64.4 (64.4, 64.4)
MEI	0.22 (0.05, 0.40)	0.35 (0.10, 1.00)	−1.2 (−2.7, −0.7)
NIÑO34	0.21 (0.05, 0.39)	0.34 (0.13, 1.00)	−1.5 (−2.8, −0.8)
DMI	0.22 (0.05, 0.41)	0.47 (0.04, 1.00)	−0.9 (−1.5, −0.1)
GPCP	0.11 (0.01, 0.26)	0.52 (0.02, 1.00)	55 (29, 83)
GPCP2	0.18 (0.05, 0.35)	0.91 (0.05, 1.00)	122 (103, 156)
GPCP3	0.29 (0.13, 0.46)	0.93 (0.12, 1.00)	285 (254, 337)
GPCP4	0.32 (0.17, 0.50)	0.96 (0.13, 1.00)	322 (279, 333)
GPCP5	0.35 (0.18, 0.54)	0.99 (0.12, 1.00)	531 (503, 536)
GPCP6	0.32 (0.14, 0.52)	0.91 (0.39, 1.00)	803 (564, 905)
PRECL	0.15 (0.04, 0.29)	0.03 (0.01, 0.08)	NA
PRECL2	0.20 (0.08, 0.34)	0.04 (0.01, 0.11)	NA
PRECL3	0.25 (0.12, 0.40)	0.04 (0.02, 0.22)	NA
PRECL4	0.26 (0.13, 0.42)	0.04 (0.02, 0.10)	NA
PRECL5	0.25 (0.11, 0.42)	0.04 (0.02, 0.10)	NA
PRECL6	0.22 (0.08, 0.39)	0.04 (0.01, 0.10)	NA
SOILM	0.24 (0.11, 0.39)	0.04 (0.01, 0.09)	NA
PDSI	0.06 (0.01, 0.15)	0.01 (0.00, 0.03)	−51 (−99, 55)

[a] R^2 values for log linear fit, R^2 values for piecewise fit, threshold estimate α for piecewise fit. Values in parentheses indicate bootstrap-derived 95% confidence intervals. NA, not available.

well constrained than under the simpler log linear model. The exception was for the GPCP4 predictor, which had a high and well-constrained R^2 of 0.97. The threshold estimate for this predictor was 317 mm, above which severe burning was largely absent (Figure 6). In SSUM, the SOILM performed substantially better than the PDSI for both the log linear and piecewise models, whereas in CSUM and EQSA the results were poor for both soil moisture models.

[30] The biggest gains in predictability for a subregional analysis were for the SKAL region (Table 5), the largest region in terms of area and total emissions. The best overall predictor was GPCP4, which had a well-constrained R^2 of 0.92 under the piecewise model. The GPCP3 performed comparably, with an R^2 of 0.88. The fitted model in this case performs well in capturing the 208 Tg of emissions in September 1997, the single largest emissions month across all regions (Figure 7). The estimated GPCP4 threshold of 595 mm does an excellent job in distinguishing severe haze months, and the magnitude of this index corresponds to that of the emissions for the 1997, 2002, and 2006 periods. Over SKAL, the precipitation-based variables performed significantly better than any of the ENSO-based indices, the best of which was the DMI with an R^2 of 0.44. Like in SSUM, the SOILM model outperformed the PDSI, showing potential usefulness on a limited regional basis.

[31] For reference, Figure 8 shows the fitted piecewise and log linear models for GPCP4, showing the advantage of the former's threshold-based approach. Under the log linear model, the gradual increase in C emissions with decreasing precipitation gives no impression of a distinction between severe and nonsevere burning periods. Converesly, this distinction is explicit under the piecewise model below a GPCP4 threshold of 595 mm. The linear segment above the threshold more appropriately captures the lack of variability in C emissions above the threshold, whereas this variability is inflated under the log linear model, leading to its weaker fit.

[32] In EKAL, the GPCP2 and GPCP3 under a log linear model were the best predictors, with R^2 = 0.60 and R^2 = 0.61, respectively (Table 6). Values under the piecewise model were lower and had higher uncertainty, with a maximum R^2 of 0.58 for the GPCP2 index and a corresponding threshold estimate of 171 mm. The threshold estimate does, however, distinguish between the burning and nonburning periods (Figure 9), although not between magnitudes of the 1997 burning and the much larger 1998 burning. In PAP, the GPCP5 index was the best log linear predictor with an R^2 of 0.35, but generally low compared to other regions (Table 7). The GPCP6 under the piecewise model had a somewhat constrained R^2 of 0.91 corresponding to a threshold of 803 mm (Figure 10). The piecewise estimates for EKAL and PAP were unique in that, whereas the PRECL R^2 estimates were all near 0, the best GPCP estimates indicated some level of predictability under the piecewise model,

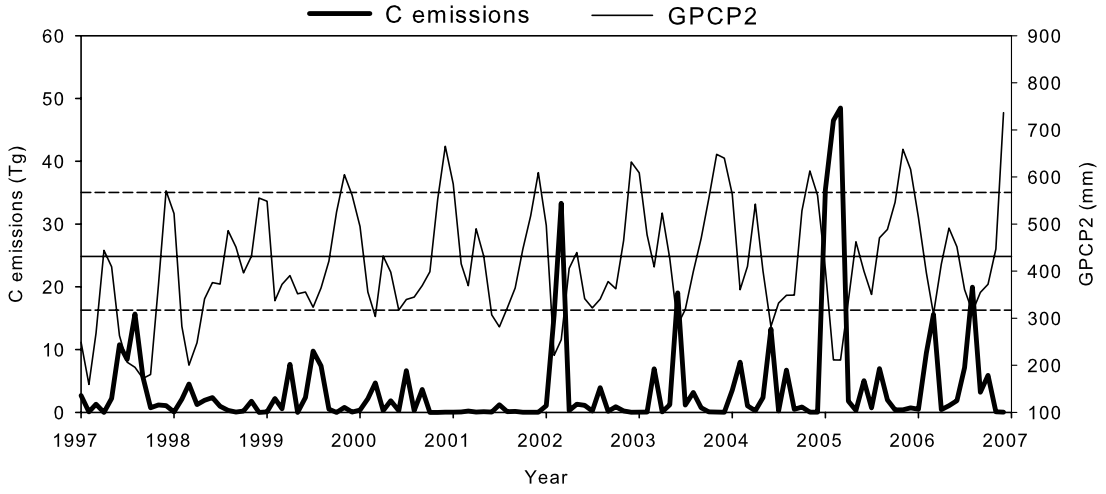

Figure 5. CSUM monthly C emissions and GPCP2. The solid horizontal line is the threshold estimate, and the dashed lines are 95% confidence intervals.

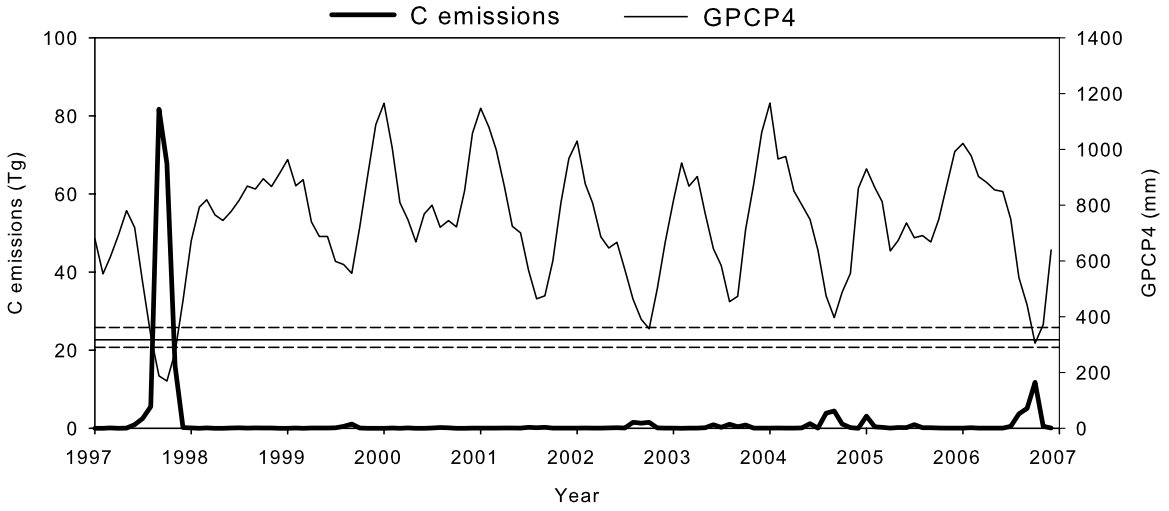

Figure 6. SSUM monthly C emissions and GPCP4. The solid horizontal line is the threshold estimate, and the dashed lines are 95% confidence intervals.

albeit with considerable uncertainty. This can likely be explained by the scarcity of ground-based stations in both regions in the PRECL data set, and hence, the improvement yielded by the incorporation of satellite data, similar to the SKAL region.

4. Discussion

4.1. Summary of Drought-Fire Predictability

[33] The rainfall-based indices performed significantly better across all regions than the SST-based predictors, and in some cases could explain a large proportion of the variance in C emissions. Across the entire EQSA analysis domain, the gauge-based PRECL and hybrid gauge-satellite GPCP indices had comparable performance. The station density across this large area appears sufficient to warrant use of a gauge-based index only, although there was no disadvantage in the inclusion of satellite-based data. In the case of both the PRECL and GPCP, the predictability of C using a spatial precipitation average over such a large area was surprisingly good, given the heterogeneity in precipitation seasonality between regions, the inclusion of regions largely absent of fire such as Sulawesi and Java, and in the case of the GPCP, the inclusion of nonland regions.

[34] In SSUM, the incorporation of satellite data provided only small advantages over the PRECL indices, perhaps reflecting a more even station distribution or greater proximity of stations to burning regions. For the SKAL subregion, the incorporation of satellite data into the GPCP yielded significant improvements in C emissions predictability. This was also the case in EKAL and PAP under the log linear models where the GPCP R^2 values were consistently higher than for the PRECL indices.

[35] In none of the regions did the SOILM model perform better than the rainfall indices, and the PDSI consistently had no power in predicting C emissions. The PDSI performed poorly due to the fact that it is an anomaly based index, reflecting departures from normal precipitation levels. Fuel moisture, conversely, is controlled by absolute

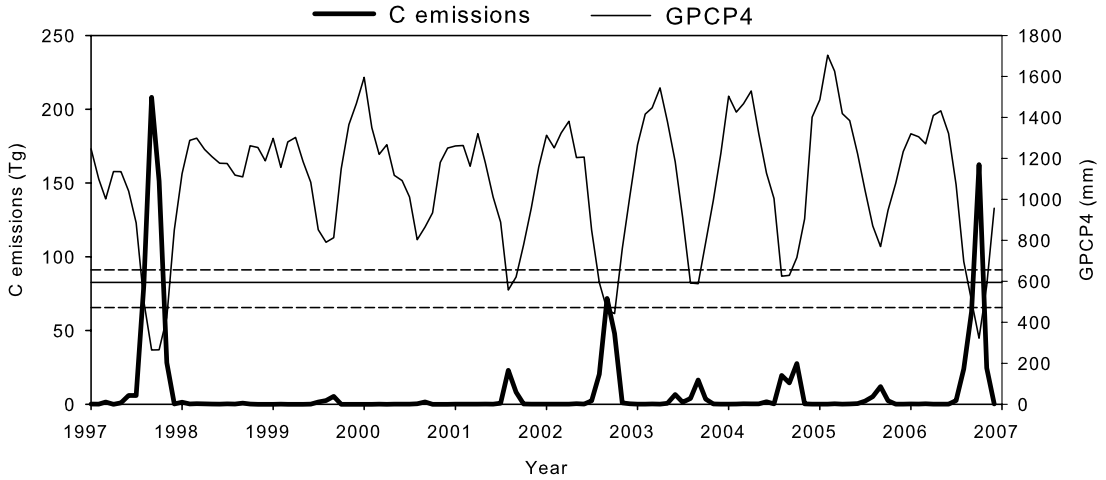

Figure 7. SKAL monthly C emissions and GPCP4. The solid horizontal line is the threshold estimate, and the dashed lines are 95% confidence intervals.

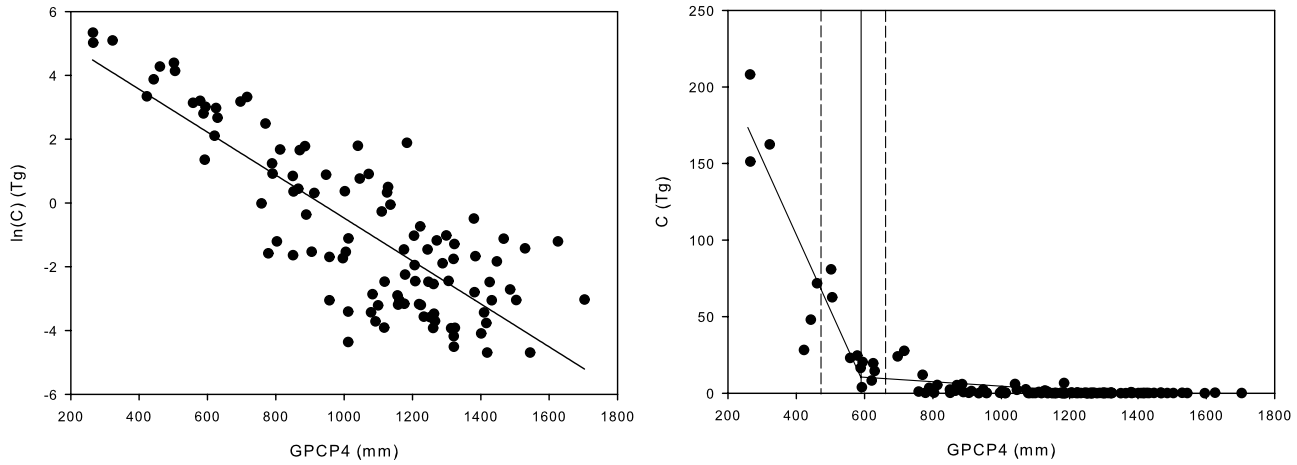

Figure 8. (left) Log linear and (right) piecewise fits for SKAL with GPCP4 predictor.

precipitation amounts. In Indonesia, even during a wet season with anomalously low precipitation, there is still sufficient precipitation to saturate peat soils, an effect which is not captured by the PDSI. To confirm this, we repeated all regressions using PRECL and GPCP monthly total anomalies, and found that their performance was uniformly poorer than the regressions for the absolute precipitation totals.

[36] Fire occurrence in CSUM, and to some extent EKAL, proved more difficult to predict, which was similar to the results of *van der Werf et al.* [2008]. In their study, cell-by-cell correlations were computed between TRMM hot spot occurrence and a seasonal fire danger index for 1998 to 2006. Strong positive correlations were observed between hot spot counts and fire danger in the SSUM and SKAL regions, but were absent or weakly negative in CSUM and EKAL. We note that both the CSUM and EKAL fall outside of Indonesia's primary rainfall region, as defined by *Aldrian and Susanto* [2003], who showed that both regions experience two shorter dry seasons, due to the twice annual absence of the ITCZ. This is seen most clearly in the GPCP2 signal for CSUM (Figure 5), which exhibits a second mode of higher frequency variability not seen in other regions. In EKAL (Figure 9), the early 1998 drought was unique compared to other regions where normal northwest monsoon precipitation was present, confirming the results of *Field et al.* [2004].

[37] In contrast, a more pronounced single dry season occurs across SSUM and SKAL when the Intertropical Convergence Zone (ITCZ) is positioned to the north. The lack of fire predictability over CSUM could partly be explained by the lack of a single persistent dry season to more narrowly restrict agricultural burning activities. Other nonclimatic factors such as differences in peat drainage are also potential explanations which require further investigation.

[38] Overall, in wanting to identify a single common index, we suggest that the GPCP4 is appropriate for SSUM and SKAL, where predictability was robust. In the case of SSUM, a 4-month rainfall total of less than 350 mm would indicate the potential for serious haze, as would a 4-month precipitation total of less than 650 mm in SKAL. In PAP, serious haze occurred only in 1997 and was associated with a rainfall threshold of 900 mm.

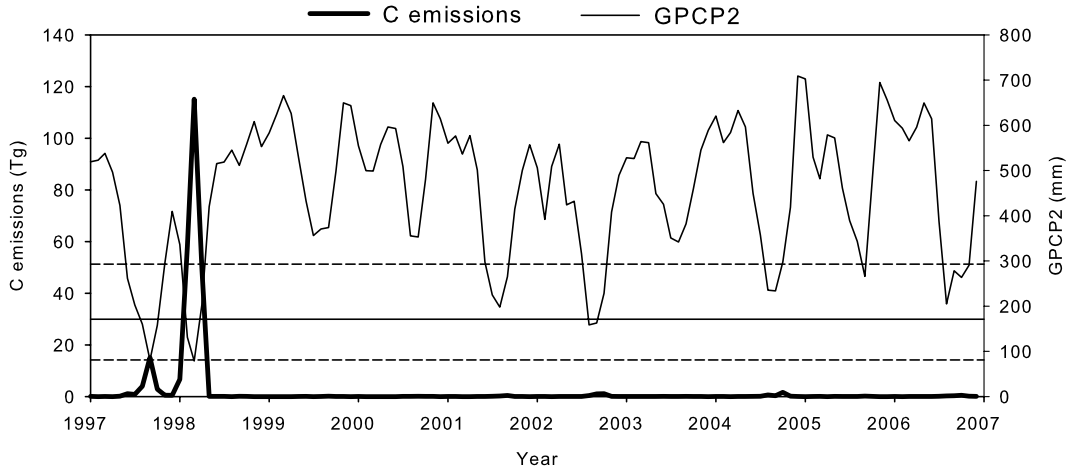

Figure 9. EKAL monthly C emissions and GPCP2. The solid horizontal line is the threshold estimate, and the dashed lines are 95% confidence intervals.

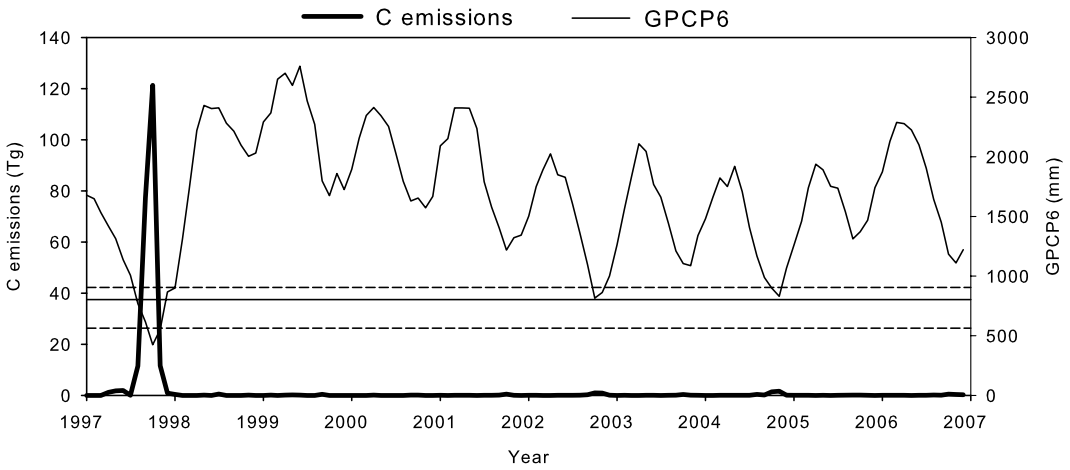

Figure 10. PAP monthly C emissions and GPCP6. The solid horizontal line is the threshold estimate, and the dashed lines are 95% confidence intervals.

[39] The predictability of fire obtained in this analysis is stronger than previous studies of Indonesia and comparable regions. Over all of Indonesia, the predictability of C emissions from the SOI and Niño3.4 was limited, consistent with the results of *Fuller and Murphy* [2006]. During their analysis period of July 1996 to December 2001, the R^2 of the log linear relationship was $R^2 = 0.46$ for both the SOI and Niño3.4 for predicting C emissions, nearly identical to their R^2 for counts of ATSR hot spot and the SOI ($R^2 = 0.46$) and Niño3.4 ($R^2 = 0.49$). This is unsurprising given

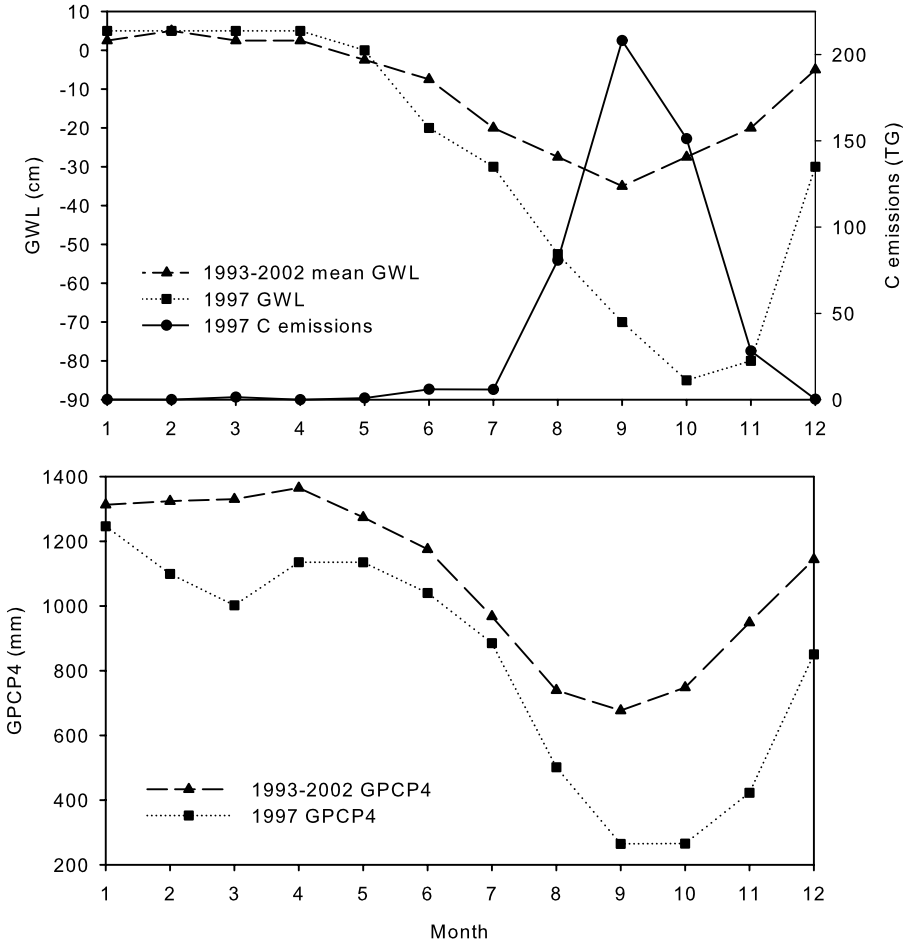

Figure 11. (top) Groundwater levels near Palangka Raya, central Kalimantan from *Usup et al.* [2004] with GFED C emissions from SKAL. (bottom) GPCP4 totals over SKAL.

that GFED data is based in large part on ATSR fire counts. During the 1997–2006 period considered in our study, however, the SOI and Niño3.4 had R^2 values of 0.27 and 0.28, respectively, both with considerable uncertainty. The Fuller and Murphy result was applicable, as suggested by them, only to the strong 1997/1998 El Niño cycle and subsequent few years.

[40] For peatlands in western Canada, *Turetsky et al.* [2004] showed that large fires occurred under warmer and drier conditions, but that a series of climatic indices under a multivariate statistical model could only explain 9% of the variation in fire size. For their more intensive study region in central Alberta, a maximum of 40% of the variability in fire size could be explained by climatic factors. *Dolling et al.* [2005] showed that over the Hawaiian islands, the maximum predictability across all islands using the Keetch-Byram Drought Index was 18% for both burned area and for total number of fires. We propose that the stronger predictability in Indonesia is due to fire being strictly human caused. In temperate regions, fire management agencies are heavily invested in fire prevention and suppression programs, which under drought conditions will help to limit the number and size of fires. Furthermore, a large proportion of ignitions are caused by lightning, which occurs irregularly and not necessarily in drought regions. In Indonesia, by contrast, burning is relied upon as a land clearing tool and will likely occur whenever conditions are sufficiently dry.

4.2. Precipitation Controls on Peat Fuel Availability

[41] Previous studies have shown that the majority of emissions in Indonesia result from peat burning, and not from surface fuel burning [*Levine*, 1999; *Page et al.*, 2002]. While the fuel moisture of dead alang-alang grass and agricultural residues will be influenced by precipitation, fires in these fuel types are important mainly in providing an ignition source for fires which spread below into peat.

[42] Physically, the seasonal precipitation considered here controls water table depth, which controls the amount of peat able to dry, and hence the fuel available for combustion. There are no comprehensive field observations of water table depth across Indonesia, but some field data have been collected. *Usup et al.* [2004] monitored water table depth from 1993 to September 2002 for a peat swamp in Central Kalimantan within our SKAL domain. Figure 11 shows the monthly groundwater level (GWL) at their study site, GFED C emissions for SKAL, and GPCP4 total for the 1993–2002 period and the 1997 drought. On average over the 1993–2002 period, groundwater levels reached an annual minimum of 35 cm below the surface in September, slowly recovering to surface levels during the remainder of the year. The situation in 1997 was much different. Beginning in June, groundwater levels began to depart from climatological levels, but were only 10 cm below normal levels for June and July. This difference widened in August, with groundwater level of 53 cm, twice the normal depth, at which time the severe burning started. Groundwater levels continued to decrease through September (70 cm), reaching a minimum in October of 85 cm, compared to a climatological average of 28 cm. September and October were also when C emissions were most severe. Groundwater levels began to slowly recover in November, reaching a depth of 30 cm in December, at which point burning had stopped. Postfire measurements in the same region made by *Page et al.* [2002] showed a mean depth of burn of 50 cm during 1997, presumably the depth to which sufficient drying had occurred to sustain peat combustion.

[43] The difference between climatological and 1997 groundwater levels is very well captured by the GPCP4 totals over SKAL. On average, the GPCP4 begins to decrease in May, and reaches a minimum of 677 mm in September, increasing through the remainder of the year to 1144 mm in December. In 1997, the GPCP4 July total of 885 mm was only slightly lower than its climatological normal, but dropped sharply to 502 mm in August, well below the estimated threshold of 595 mm. This decrease continued into September, during which only 33 mm of precipitation occurred, and remained low through October at 265 mm, slowly recovering through November, and crossing above the threshold in December with the delayed arrival of the northwest monsoon. We note that the 1997 groundwater levels are nearly perfectly correlated with the GPCP4 (R^2 = 0.93), much greater than with the single month GPCP (R^2 = 0.51), providing physical evidence of how the variation in back totaled precipitation reflects the cumulative nature of water table depth on the landscape.

[44] The estimated threshold is also relevant for severe burning during the 1994 haze episode. The water table at a site in central Kalimantan near that of *Usup et al.* [2004] reached a minimum depth of roughly 75 cm in October and November of 1994 [*Jauhiainen et al.*, 2005] corresponding to a 4-month GPCP October total of 239 mm over SKAL. Although this predates the GFED data, severe fires were known to occur during this period, generating regional haze across western Indonesia, Singapore and Peninsular Malaysia [*Nichol*, 1997; *Yonemura et al.*, 2002; *Field et al.*, 2004].

[45] In Sumatra, where GPCP4 was the best predictor, the lower threshold of 317 mm indicates a less sensitive fire environment, with severe fire events occurring only during more severe droughts than in SKAL. It is not immediately clear why this would be the case, although perhaps the peatlands have undergone less drainage, which seems less likely than there simply being less agricultural activity and consequent burning during the past decade in SSUM compared to SKAL.

[46] The PAP region also appears to have a less sensitive fire environment than SKAL, with the longer-term GPCP6 being the best predictor of C emissions, rather than the GPCP4. PAP's only severe fire event occurred in 1997, although climatologically low GPCP6 values also occurred during the dry seasons of 2002 and 2004. The simplest explanation is that PAP has undergone less forest degradation, and so is less subject to severe fires.

4.3. Spatial Drought Patterns and Underlying Sea Surface Temperature Controls

[47] Although the SST-based predictors did not perform as well as the precipitation-based indicators, they did offer some level of predictability of C emissions which varied meridionally across Indonesia. Under the piecewise model, there is an apparent decrease from west to east in the influence of Indian Ocean SSTs and an increase in that of Pacific SSTs on C emissions. Over SSUM the DMI explained 50% of the variance in C emissions, compared to 35% explained by the

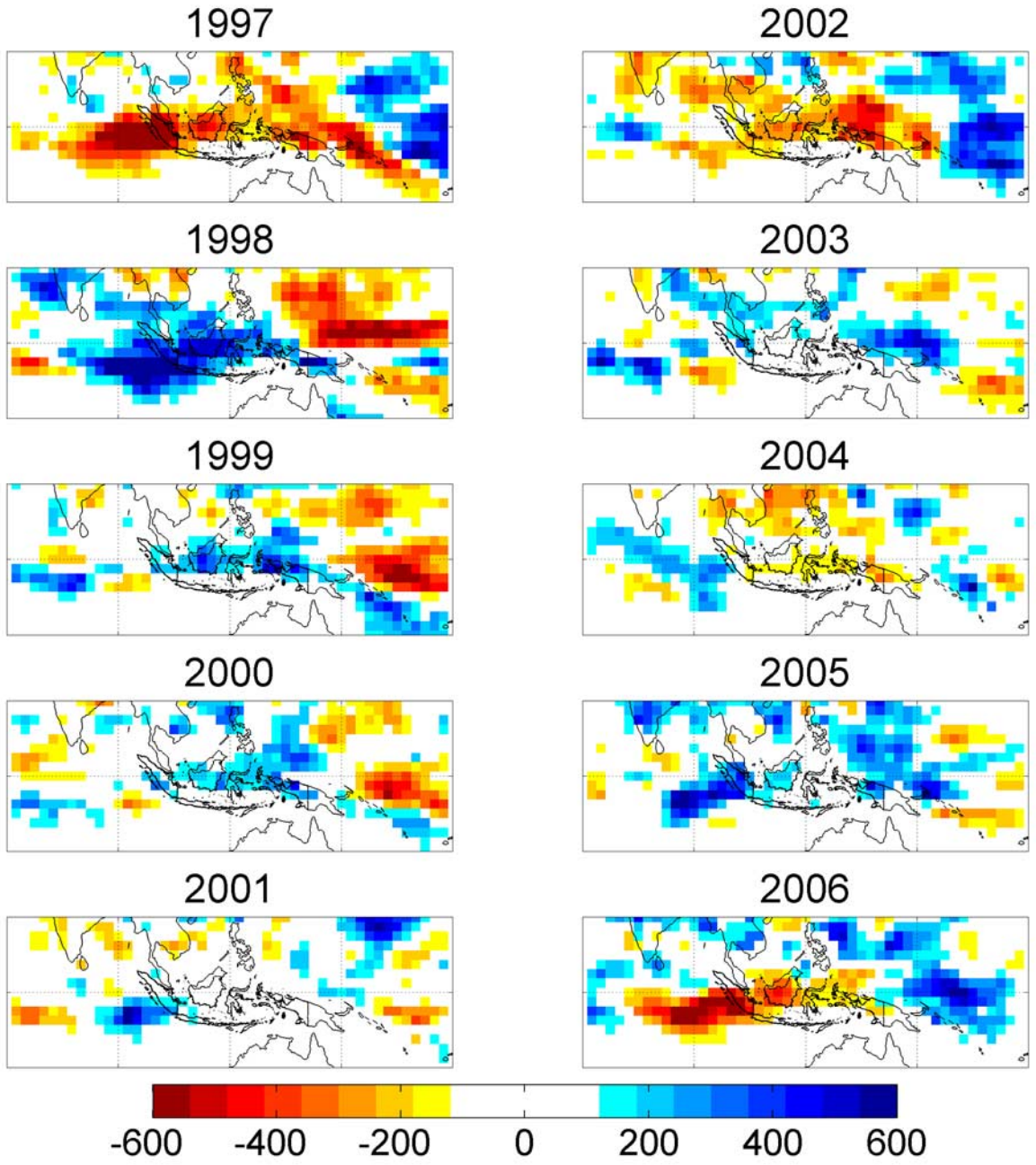

Figure 12. October GPCP4 totals (mm) for 1997 to 2006.

Niño3.4. Over SKAL, 44% of variance in C emissions is explained by the DMI, compared to 23% by the Niño3.4. In EKAL, which is in a separate rainfall zone as defined by *Aldrian and Susanto* [2003], the MEI explained 46% of the C emissions variability, compared to only 1% explained by the DMI. PAP was similar, where the DMI was not well constrained, but the Niño3.4 had a somewhat well-constrained predictability at 34%.

[48] Any SST control on C emissions occurs via the former's control on atmospheric circulation and precipitation over Indonesia. Detailed investigations on these precipitation controls have been made by others [*Saji et al.*, 1999; *Hendon*, 2003; *Juneng and Tangang*, 2005] and were beyond the scope of our analysis, but we did wish to distinguish between the nature of different drought episodes over Indonesia with respect to seasonal precipitation and underlying SST patterns.

[49] GPCP4 anomaly maps for October for 1997 through 2006 are shown in Figure 12. The 1997 dry conditions over Indonesia can be seen as part of a larger region of anomalously low precipitation spanning the central eastern Indian Ocean in the west to the Solomon Islands in the east. This dry region is bounded by normal precipitation amounts to the north and south and a strong positive precipitation anomaly to the east, corresponding to the eastward shifted position of the Walker circulation's terminal convective

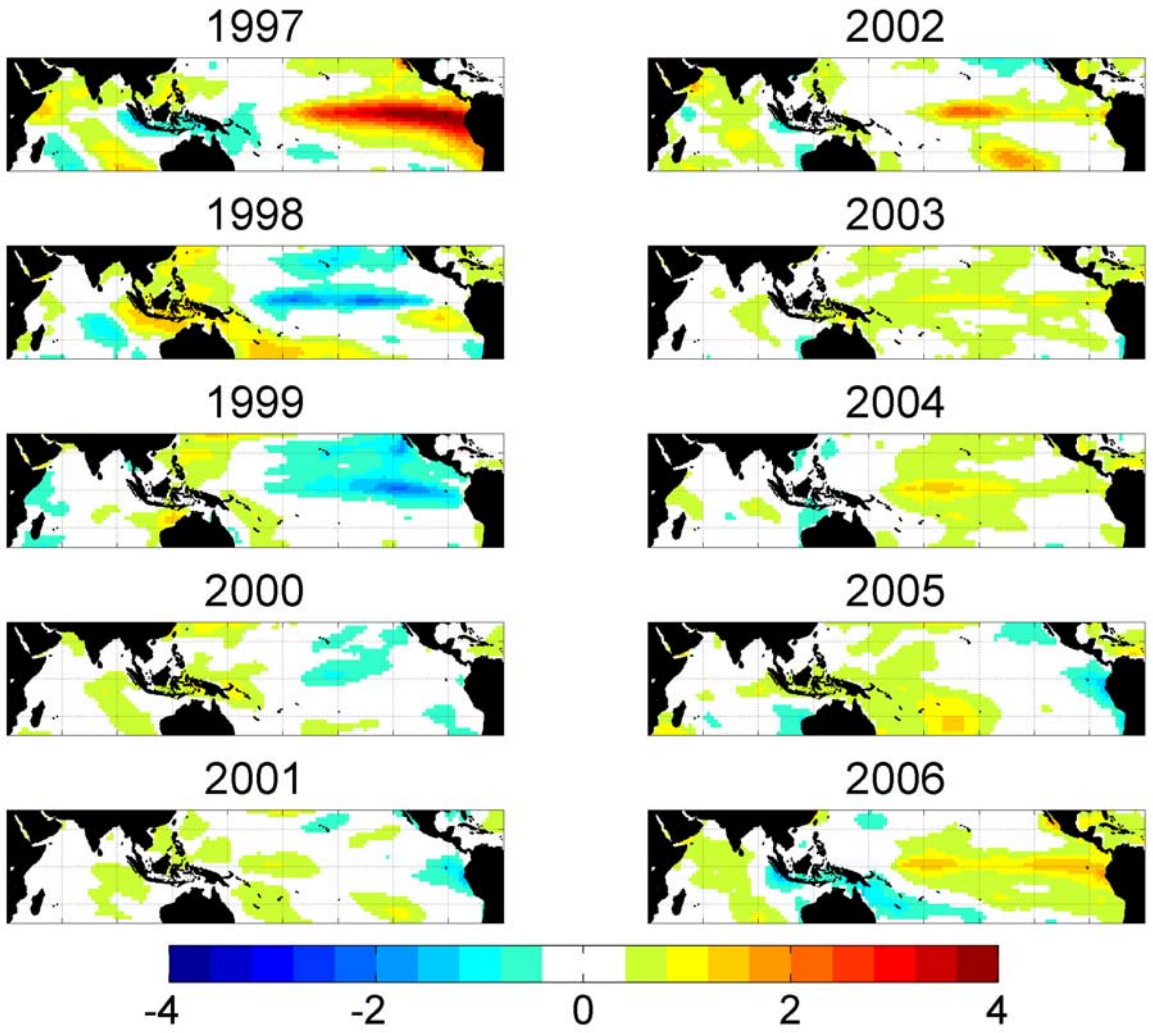

Figure 13. October SST anomalies (°C) over the Indian and tropical Pacific oceans from 1997 to 2006 [*Reynolds et al.*, 2002].

branch. The 1997 event illustrates the sharp distinction between normal and anomalously low regions of precipitation: the pronounced drought conditions seen over Sumatra and Kalimantan were absent over the Java Sea, the island of Java, southern Sulawesi and the Lesser Sunda Islands stretching to East Timor.

[50] In 1998, conditions over Indonesia had reversed, with a wet precipitation anomaly over Indonesia of roughly the same absolute magnitude as the dry anomaly in 1997. Weaker positive precipitation anomalies persisted over the region in 1999 and 2000, with near-neutral conditions in 2001. During the moderate El Niño conditions of 2002, there was a moderate dry anomaly over Indonesia which was most pronounced to the north of Papua, and appearing only weakly over Sumatra and Kalimantan. The less severe burning during 2002 was therefore due to relocation of the drought center, rather than by the actual absence of severe drought.

[51] Wet-neutral conditions occurred in 2003 and dry-neutral conditions in 2004, the weaker anomaly corresponding to relatively weak El Niño conditions, but also to the positioning of the main drought center over the South China Sea rather than western Indonesia. 2005 saw wet-neutral conditions over central Indonesia, bounded by strong wet regions to the east and west. The pronounced dry anomaly of 2006 was closer in nature to that of 1997 but limited in extent to Kalimantan, Sumatra and the Indian Ocean between 75E and 100E and 0 to 15S. There is therefore considerable spatial variability of drought over in Indonesia, which further explains why subregional prediction of fire occurrence performed better than that across the entire EQSA region.

[52] The stronger precipitation anomalies in 1997 and 2006 over SSUM and SKAL appear driven by the combined effects of SST anomalies in the Pacific and Indian Ocean basins. Figure 13 shows global mean SST anomalies between 1997 and 2006 for October, when the greatest dry GPCP4 anomalies would occur. The large 1997 El Niño event is seen clearly, with the strongest eastern Pacific warm SST anomaly seen during our analysis period. Similar anomalies but of weaker magnitude were also seen during 2002 and to a lesser extent in 2006.

[53] Common to both 1997 and 2006, but only weakly present in 2002 and absent during all other years, is a

negative SST anomaly in the Indian Ocean off of the coasts of western Sumatra and the southern coast of Java, coupled with above average SSTs in the western Indian Ocean, reflected by the elevated DMI values. *Saji et al.* [1999] proposed that this pattern induces anomalously low precipitation in western Indonesia via the following mechanism. The cooler than normal SSTs weaken the southeasterly trades in the southeastern Indian Ocean, shifting equatorial convergence to the northwest of its normal position in the Indian Ocean. As a result, the equatorial westerlies in the Indian Ocean weaken, suppressing heat supply to and convergence over western Indonesia, and ultimately, contributing to reduced precipitation. This was consistent with *Hendon*'s [2003] analysis, which showed that precipitation over all of Indonesia was negatively correlated with SSTs in the southeastern Indian Ocean.

[54] This could explain why none of Indian or Pacific Ocean based indices were individually able to explain beyond 50% of C emissions variability; each of the droughts occurred for different reasons. The severity and large spatial extent of the 1997 drought resulted from weaker atmospheric flow from both the east from the Pacific Ocean and from the southwest from the Indian Ocean, resulting in weaker convergence over all of Indonesia. The 2002 drought, which was most severe in eastern Indonesia, was the result of reduced flux from the Pacific Ocean, whereas the 2006 drought, most pronounced over western Indonesia, was the result of reduced flux from the Indian Ocean. The enhanced biomass burning in 2006 over Indonesia therefore seems less attributable to the moderate El Niño, and more to the concurrent IOD event. Similarly, the significant drought and fire in 1994 [*Nichol*, 1997; *Fujiwara et al.*, 1999; *Yonemura et al.*, 2002; *Field et al.*, 2004] occurred under El Niño conditions weaker than in 2002, but under strongly positive DMI conditions [*Saji et al.*, 1999]. Overall, the Indian Ocean SSTs appear to have a comparable, if not greater, effect on west Indonesian drought than Pacific Ocean SSTs.

4.4. Future Drought Conditions

[55] In the absence of peatland restoration and management, any future rainfall decrease in Indonesia's peatland regions caused by climate change would increase fire danger and result in increased C emissions. The most acute risks are posed by an increase in the frequency at which the seasonal precipitation thresholds estimated here, and hence peat moisture levels, are crossed. This could be caused by an increase in higher frequency of El Niño or Indian Ocean Dipole events, or a decrease in normal condition dry season precipitation toward below threshold values.

[56] Climate change projections of precipitation over Indonesia remain inconclusive, but allow for the possibility of a decrease in certain regions. The IPCC AR4 projections of precipitation changes over Indonesia showed little agreement between models in the sign of any change, but this was an examination only DJF and JJA precipitation, whereas the most critical changes in Indonesia involve a prolonged dry season through the SON period. *Li et al.* [2007] considered rainfall over western Indonesia during the more relevant JAS period under the IPCC SRES A1B anthropogenic emissions scenario. Rainfall was seen to decrease for 7 of the 11 models considered, particularly south of the equator, which they translated into an increase in water table depth and increased evaporative fraction (ratio of latent heat flux to net evaporation). Such a change in mean state of Indonesia's peatland hydrology would increase the susceptibility to deep peat fires and further C emissions.

[57] As shown in Figure 12, the 1997 and 2006 droughts were most pronounced over the Indian Ocean to the west of Sumatra and not over the Indonesian islands. We would argue that any persistent eastward shift in this drought center, which seems most closely related to IOD events, represents the greatest possible increase in Indonesian fire danger.

5. Summary and Conclusions

[58] We have shown that a large portion of the emissions from biomass burning in Indonesia are controlled by drought, which is best characterized by simple rainfall totals as opposed to more complicated soil moisture models or SST indices. It should come as no surprise that fire susceptibility in Indonesia is better explained by regional precipitation than by SST or pressure-based climate indices. This analysis has helped to quantify the extent to which this is the case, and will hopefully lead to better operational fire management planning to reduce future emissions episodes. Indeed, the effectiveness of SST indices in predicting fire occurrence is limited by the strength of their control on regional precipitation, which in turn is the physical underlying trigger for the burning through its control of groundwater levels in Indonesia's peatlands.

[59] None of the SST-based indices considered here can individually explain drought occurrence over Indonesia, which can vary spatially and result from anomalies in either or both of the Pacific or Indian Ocean basins. Caution should therefore be exercised when attributing Indonesian fire and drought events to a single cause such as El Niño. Other historical studies [*Kita et al.*, 2000; *Wang et al.*, 2004] attributing fire episodes strictly to El Niño conditions appear to have oversimplified controlling factors on fire occurrence; it would be worthwhile revisiting these analyses to determine the relative contributions of SST variability in the Pacific and Indian oceans to drought and fire over Indonesia.

[60] Significant improvements were gained in predicting fire occurrence by considering rainfall within a specific region, compared to precipitation across all of Indonesia. Precipitation and drought are too spatially variable over Indonesia to be meaningfully quantified by a single drought indicator. For southern Sumatra and southern Kalimantan, region-specific analysis allowed for the estimation of precipitation thresholds suitable for distinguishing between periods of low and high fire danger. A piecewise regression model provided a means of estimating this threshold objectively, and nonparametric bootstrapping was useful in providing confidence limits for predictability and threshold estimates. The piecewise model also allowed us to avoid the variance-inflating properties of a log linear model and the unclear physical interpretation of log-transformed C emissions. Precipitation estimates derived from remote sensing products appear to have an advantage over strictly gauge-based products in characterizing the threshold-driven nature

of the fire response to drought, particularly in southern Kalimantan.

[61] The daily drought indices considered by *Sudiana et al.* [2003], *Field et al.* [2004], and *Dymond et al.* [2005] are appropriate, with local calibration, for operational fire danger monitoring. The monthly precipitation totals considered here can complement those indices, and provide more readily interpretable guidelines against which to interpret seasonal rainfall outlooks provided from statistical or ensembles of numerical weather prediction model integrations, such as those described by *van Oldenborgh et al.* [2005]. Such thresholds can also serve as benchmark against which to assess possible future reductions in rainfall during the dry season over Sumatra and Kalimantan under a changing climate.

[62] This analysis was based on 10 years worth of data, with only a few periods of severe biomass burning. As in the work by *Fuller and Murphy* [2006] and *van der Werf et al.* [2008], this made the robustness of our estimates difficult to assess, and resulted in wide confidence intervals for most R^2 values under the piecewise model. Every effort should be made to extend the fire occurrence record back in time, perhaps by incorporating AVHRR data, following *Sudiana et al.* [2003]. In the future, we hope to extend this type of analysis to the 1970s using observations of visible range at airports, which were used as a haze indicator by *Wang et al.* [2004] over Sumatra from 1973 to 2003. The start of this period coincided with that of Indonesia's official transmigration policies and increased development in the fire prone areas of Sumatra and Kalimantan [*Fearnside*, 1997], and could help to separate the influence of natural interannual rainfall variability from anthropogenic land cover disturbance, and to further constrain estimates of predictability and drought thresholds. Further to this, the threshold-driven nature of severe burning needs to be considered in the context of possible positive feedbacks between deforestation, precipitation and fire [*Siegert et al.*, 2001; *Cochrane*, 2003; *Hoffmann et al.*, 2003], and between black carbon emissions, increases in atmospheric stability and reduced precipitation [*Koren et al.*, 2004; *Liu*, 2005].

[63] **Acknowledgments.** We thank Christine Lee, Ray Nassar, and two anonymous reviewers for valuable comments and Guido van der Werf, Mingyue Chen, and Yun Fan for assistance with the data sets. R.D.F. was supported by a grant from the Southeast Asia Regional Committee for START and a graduate scholarship from the Natural Sciences and Engineering Research Council of Canada.

References

Adler, R. F., et al. (2003), The Version-2 Global Precipitation Climatology Project (GPCP) monthly precipitation analysis (1979–Present), *J. Hydrometeorol.*, *4*(6), 1147–1167, doi:10.1175/1525-7541(2003)004<1147:TVGPCP>2.0.CO;2.

Aldrian, E., and R. D. Susanto (2003), Identification of three dominant rainfall regions within Indonesia and their relationship to sea surface temperature, *Int. J. Climatol.*, *23*(12), 1435–1452, doi:10.1002/joc.950.

Chen, M. Y., P. P. Xie, J. E. Janowiak, and P. A. Arkin (2002), Global land precipitation: A 50-yr monthly analysis based on gauge observations, *J. Hydrometeorol.*, *3*(3), 249–266, doi:10.1175/1525-7541(2002)003<0249:GLPAYM>2.0.CO;2.

Cochrane, M. A. (2003), Fire science for rainforests, *Nature*, *421*(6926), 913–919, doi:10.1038/nature01437.

Dai, A., K. E. Trenberth, and T. Qian (2004), A global data set of Palmer Drought Severity Index for 1870–2002: Relationship with soil moisture and effects of surface warming, *J. Hydrometeorol.*, *5*, 1117–1130, doi:10.1175/JHM-386.1.

de Groot, W. J., Wardati, and Y. H. Wang (2005), Calibrating the fine fuel moisture code for grass ignition potential in Sumatra, Indonesia, *Int. J. Wildland Fire*, *14*(2), 161–168, doi:10.1071/WF04054.

Dennis, R. A., et al. (2005), Tomich, fire, people and pixels: Linking social science and remote sensing to understand underlying causes and impacts of fires in Indonesia, *Human Ecol.*, *33*(4), 465–504, doi:10.1007/s10745-005-5156-z.

Dolling, K., P. S. Chu, and F. Fujioka (2005), A climatological study of the Keetch/Byram Drought Index and fire activity in the Hawaiian islands, *Agric. For. Meteorol.*, *133*(1–4), 17–27, doi:10.1016/j.agrformet.2005.07.016.

Duncan, B. N., R. V. Martin, A. C. Staudt, R. Yevich, and J. A. Logan (2003), Inter-annual and seasonal variability of biomass burning emissions constrained by satellite observations, *J. Geophys. Res.*, *108*(D2), 4100, doi:10.1029/2002JD002378.

Dymond, C. C., R. D. Field, O. Roswintiarti, and Guswanto (2005), Using satellite fire detection to calibrate components of the Fire Weather Index system in Malaysia and Indonesia, *Environmental Management*, *35*(4), 426–440, doi:10.1007/s00267-003-0241-9.

Efron, B., and R. J. Tibshirani (1993), *An Introduction to the Bootstrap*, 436 pp., Chapman and Hall, Boca Raton, Fla.

Fan, Y., and H. van den Dool (2004), Climate Prediction Center global monthly soil moisture data set at 0.5° resolution for 1948 to present, *J. Geophys. Res.*, *109*, D10102, doi:10.1029/2003JD004345.

Fearnside, P. M. (1997), Transmigration in Indonesia: Lessons from its environmental and social impacts, *Environ. Manage. N. Y.*, *21*(4), 553–570, doi:10.1007/s002679900049.

Field, R. D., Y. Wang, O. Roswintiarti, and Guswanto (2004), A drought-based predictor of recent haze events in western Indonesia, *Atmos. Environ.*, *38*(13), 1869–1878, doi:10.1016/j.atmosenv.2004.01.011.

Frandsen, W. H. (1997), Ignition probability of organic soils, *Can. J. For. Res.*, *27*(9), 1471–1477, doi:10.1139/cjfr-27-9-1471.

Fujiwara, M., K. Kita, S. Kawakami, T. Ogawa, N. Komala, S. Saraspriya, and A. Suripto (1999), Tropospheric ozone enhancements during the Indonesian forest fire events in 1994 and in 1997 as revealed by ground-based observations, *Geophys. Res. Lett.*, *26*(16), 2417–2420, doi:10.1029/1999GL900117.

Fuller, D. O., and K. Murphy (2006), The ENSO-fire dynamic in insular Southeast Asia, *Clim. Change*, *74*(4), 435–455, doi:10.1007/s10584-006-0432-5.

Gedalof, Z., D. L. Peterson, and N. J. Mantua (2005), Atmospheric, climatic and ecological controls on extreme wildfire years in the northwestern United States, *Ecol. Appl.*, *15*(1), 154–174, doi:10.1890/03-5116.

Gutman, G., I. Csiszar, and P. Romanov (2000), Using NOAA/AVHRR products to monitor El Nino impacts: Focus on Indonesia in 1997–98, *Bull. Am. Meteorol. Soc.*, *81*(6), 1189–1205, doi:10.1175/1520-0477(2000)081<1189:UNPTME>2.3.CO;2.

Heil, A., and J. G. Goldammer (2001), Smoke-haze pollution: A review of the 1997 episode in Southeast Asia, *Reg. Environ. Change*, *2*, 24–37, doi:10.1007/s101130100021.

Hendon, H. H. (2003), Indonesian rainfall variability: Impacts of ENSO and local air-sea interaction, *J. Clim.*, *16*(11), 1775–1790, doi:10.1175/1520-0442(2003)016<1775:IRVIOE>2.0.CO;2.

Herman, J. R., P. K. Bhartia, O. Torres, C. Hsu, C. Seftor, and E. Celarier (1997), Global distribution of UV-absorbing aerosols from Nimbus 7/TOMS data, *J. Geophys. Res.*, *102*(D14), 16,911–16,922, doi:10.1029/96JD03680.

Hessl, A. E., D. McKenzie, and R. Schellhaas (2004), Drought and Pacific Decadal Oscillation linked to fire occurrence in the inland Pacific Northwest, *Ecol. Appl.*, *14*(2), 425–442, doi:10.1890/03-5019.

Hoffmann, W. A., W. Schroeder, and R. B. Jackson (2003), Regional feedbacks among fire, climate, and tropical deforestation, *J. Geophys. Res.*, *108*(D23), 4721, doi:10.1029/2003JD003494.

Jauhiainen, J., H. Takahashi, J. E. P. Heikkinen, P. J. Martikainen, and H. Vasander (2005), Carbon fluxes from a tropical peat swamp forest floor, *Global Change Biol.*, *11*(10), 1788–1797, doi:10.1111/j.1365-2486.2005.001031.x.

Juneng, L., and F. T. Tangang (2005), Evolution of ENSO-related rainfall anomalies in Southeast Asia region and its relationship with atmosphere-ocean variations in Indo-Pacific sector, *Clim. Dyn.*, *25*(4), 337–350, doi:10.1007/s00382-005-0031-6.

Kalnay, E., et al. (1996), The NCEP/NCAR 40-Year Reanalysis Project, *Bull. Am. Meteorol. Soc.*, *77*(3), 437–471, doi:10.1175/1520-0477(1996)077<0437:TNYRP>2.0.CO;2.

Kita, K., M. Fujiwara, and S. Kawakami (2000), Total ozone increase associated with forest fires over the Indonesian region and its relation to the El Niño–Southern Oscillation, *Atmos. Environ.*, *34*(17), 2681–2690, doi:10.1016/S1352-2310(99)00522-1.

Koren, I., Y. J. Kaufman, L. A. Remer, and J. V. Martins (2004), Measurement of the effect of Amazon smoke on inhibition of cloud formation, *Science*, *303*(5662), 1342–1345, doi:10.1126/science.1089424.

Kunii, O., S. Kanagawa, I. Yajima, Y. Hisamatsu, S. Yamamura, T. Amagai, and I. T. S. Ismail (2002), The 1997 haze disaster in Indonesia: Its air quality and health effects, *Arch. Environ. Health*, *57*(1), 16–22.

Langenfelds, R. L., R. J. Francey, B. C. Pak, L. P. Steele, J. Lloyd, C. M. Trudinger, and C. E. Allison (2002), Interannual growth rate variations of atmospheric CO_2 and its $\delta^{13}C$, H_2, CH_4, and CO between 1992 and 1999 linked to biomass burning, *Global Biogeochem. Cycles*, *16*(3), 1048, doi:10.1029/2001GB001466.

Langner, A., J. Miettinen, and F. Siegert (2007), Land cover change 2002–2005 in Borneo and the role of fire derived from MODIS imagery, *Global Change Biol.*, *13*, 2329–2340, doi:10.1111/j.1365-2486.2007.01442.x.

Levine, J. S. (1999), The 1997 fires in Kalimantan and Sumatra, Indonesia: Gaseous and particulate emissions, *Geophys. Res. Lett.*, *26*(7), 815–818, doi:10.1029/1999GL900067.

Li, W., R. E. Dickinson, R. Fu, G.-Y. Niu, Z.-L. Yang, and J. G. Canadell (2007), Future precipitation changes and their implications for tropical peatlands, *Geophys. Res. Lett.*, *34*, L01403, doi:10.1029/2006GL028364.

Liu, Y. Q. (2005), Atmospheric response and feedback to radiative forcing from biomass burning in tropical South America, *Agric. For. Meteorol.*, *133*(1–4), 40–53, doi:10.1016/j.agrformet.2005.03.011.

Logan, J. A., I. Megretskaia, R. Nassar, L. T. Murray, L. Zhang, K. W. Bowman, H. M. Worden, and M. Luo (2008), Effects of the 2006 El Niño on tropospheric composition as revealed by data from the Tropospheric Emission Spectrometer (TES), *Geophys. Res. Lett.*, *35*, L03816, doi:10.1029/2007GL031698.

Lohman, D. J., D. Bickford, and N. S. Sodhi (2007), The burning issue, *Science*, *316*(5823), 376, doi:10.1126/science.1140278.

Nichol, J. (1997), Bioclimatic impacts of the 1994 smoke haze event in Southeast Asia, *Atmos. Environ.*, *31*(8), 1209–1219, doi:10.1016/S1352-2310(96)00260-9.

Ntale, H. K., and T. Y. Gan (2003), Drought indices and their application to East Africa, *Int. J. Climatol.*, *23*(11), 1335–1357, doi:10.1002/joc.931.

Page, S. E., F. Siegert, J. O. Rieley, H. D. V. Boehm, A. Jaya, and S. Limin (2002), The amount of carbon released from peat and forest fires in Indonesia during 1997, *Nature*, *420*(6911), 61–65, doi:10.1038/nature01131.

Podgorny, I. A., F. Li, and V. Ramanathan (2003), Large aerosol radiative forcing due to the 1997 Indonesian forest fire, *Geophys. Res. Lett.*, *30*(1), 1028, doi:10.1029/2002GL015979.

Reynolds, R. W., N. A. Rayner, T. M. Smith, D. C. Stokes, and W. Q. Wang (2002), An improved in-situ and satellite SST analysis for climate, *J. Clim.*, *15*(13), 1609–1625, doi:10.1175/1520-0442(2002)015<1609:AIISAS>2.0.CO;2.

Saji, N. H., B. N. Goswami, P. N. Vinayachandran, and T. Yamagata (1999), A dipole mode in the tropical Indian Ocean, *Nature*, *401*(6751), 360–363.

Sastry, N. (2002), Forest fires, air pollution, and mortality in Southeast Asia, *Demography*, *39*(1), 1–23, doi:10.1353/dem.2002.0009.

Siegert, F., and A. A. Hoffmann (2000), The 1998 forest fires in East Kalimantan (Indonesia): A quantitative evaluation using high resolution, multitemporal ERS-2 SAR images and NOAA-AVHRR hotspot data, *Remote Sens. Environ.*, *72*(1), 64–77, doi:10.1016/S0034-4257(99)00092-9.

Siegert, F., G. Ruecker, A. Hinrichs, and A. A. Hoffmann (2001), Increased damage from fires in logged forests during droughts caused by El Nino, *Nature*, *414*(6862), 437–440, doi:10.1038/35106547.

Stolle, F., and E. F. Lambin (2003), Interprovincial and inter-annual differences in the causes of land-use fires in Sumatra, Indonesia, *Environ. Conserv.*, *30*(4), 375–387, doi:10.1017/S0376892903000390.

Sudiana, D., H. Kuze, N. Takeuchiu, and R. E. Burgan (2003), Assessing forest fire potential in Kalimantan Island, Indonesia, using satellite and surface weather data, *Int. J. Wildland Fire*, *12*(2), 175–184, doi:10.1071/WF02035.

Thompson, A. M., J. C. Witte, R. D. Hudson, H. Guo, J. R. Herman, and M. Fujiwara (2001), Tropical tropospheric ozone and biomass burning, *Science*, *291*(5511), 2128–2132, doi:10.1126/science.291.5511.2128.

Toms, J. D., and M. L. Lesperance (2003), Piecewise regression: A tool for identifying ecological thresholds, *Ecology*, *84*(8), 2034–2041, doi:10.1890/02-0472.

Turetsky, M. R., B. D. Amiro, E. Bosch, and J. S. Bhatti (2004), Historical burn area in western Canadian peatlands and its relationship to fire weather indices, *Global Biogeochem. Cycles*, *18*, GB4014, doi:10.1029/2004GB002222.

Usup, A., Y. Hashimoto, H. Takahashi, and H. Hayasaka (2004), Combustion and thermal characteristics of peat fire in tropical peatland in central Kalimantan, Indonesia, *Tropics*, *14*(1), 1–19, doi:10.3759/tropics.14.1.

van der Werf, G. R., J. T. Randerson, L. Giglio, G. J. Collatz, P. S. Kasibhatla, and A. F. Arellano (2006), Inter-annual variability in global biomass burning emissions from 1997 to 2004, *Atmos. Chem. Phys.*, *6*, 3423–3441.

van der Werf, G. R., J. T. Randerson, L. Giglio, N. Gobron, and A. J. Dolman (2008), Climate controls on the variability of fires in the tropics and subtropics, *Global Biogeochem. Cycles*, *22*, GB3028, doi:10.1029/2007GB003122.

van Oldenborgh, G. J., M. A. Balmaseda, L. Ferranti, T. N. Stockdale, and D. L. T. Anderson (2005), Did the ECMWF seasonal forecast model outperform statistical ENSO forecast models over the last 15 years?, *J. Clim.*, *18*(16), 3240–3249, doi:10.1175/JCLI3420.1.

Wang, Y., R. D. Field, and O. Roswintiarti (2004), Trends in atmospheric haze induced by peat fires in Sumatra Island, Indonesia and El Niño phenomenon from 1973 to 2003, *Geophys. Res. Lett.*, *31*, L04103, doi:10.1029/2003GL018853.

Westerling, A. L., A. Gershunov, D. R. Cayan, and T. P. Barnett (2002), Long lead statistical forecasts of area burned in western US Wildfires by ecosystem province, *Int. J. Wildland Fire*, *11*(4), 257–266, doi:10.1071/WF02009.

Wolter, K., and M. S. Timlin (1993), Monitoring ENSO in COADS with a seasonally adjusted principal component index, *Rep. NOAA/N MC/CAC, NSSL*, Oklahoma Clim. Surv., CIMMS and the Sch. of Meteorol., Univ. of Okla., Norman.

Yonemura, S., H. Tsuruta, S. Kawashima, S. Sudo, L. C. Peng, L. S. Fook, Z. Johar, and M. Hayashi (2002), Tropospheric ozone climatology over Peninsular Malaysia from 1992 to 1999, *J. Geophys. Res.*, *107*(D15), 4229, doi:10.1029/2001JD000993.

Zeng, N., A. Mariotti, and P. Wetzel (2005), Terrestrial mechanisms of interannual CO_2 variability, *Global Biogeochem. Cycles*, *19*, GB1016, doi:10.1029/2004GB002273.

R. D. Field, Department of Physics, University of Toronto, 60 St. George Street, Toronto, ON M5S 1A7, Canada. (robert.field@utoronto.ca)

S. S. P. Shen, Department of Mathematics and Statistics, San Diego State University, San Diego, CA 92182, USA.